Engineering Geology 193 (2015) 61–78

Contents lists available at ScienceDirect

Engineering Geology

journal homepage: www.elsevier.com/locate/enggeo

Mapping surface deformation in open pit iron mines of Carajás Province (Amazon Region) using an integrated SAR analysis

Waldir R. Paradella [a,*], Alessandro Ferretti [b], José C. Mura [a], Davide Colombo [b], Fabio F. Gama [a], Andrea Tamburini [b], Athos R. Santos [a], Fabrizio Novali [b], Mauricio Galo [c], Paulo O. Camargo [c], Arnaldo Q. Silva [d], Guilherme G. Silva [a], Aristotelina Silva [e], Leonardo L. Gomes [e]

[a] National Institute for Space Research (INPE), São José dos Campos CEP 12227-010, Brazil
[b] Tele-Rilevamento Europa-T.R.E. Srl, 20143 Milano, Italy
[c] São Paulo State University (FCT/UNESP), Presidente Prudente CEP 19060-900, Brazil
[d] Federal University of Pará (IG/UFPA), Belém CEP 66075-110, Brazil
[e] Vale S. A. (DIFN/GEDEN/GAGHN), Serra dos Carajás CEP 68516-000, Brazil

ARTICLE INFO

Article history:
Received 12 October 2014
Received in revised form 1 April 2015
Accepted 20 April 2015
Available online 24 April 2015

Keywords:
DInSAR
TerraSAR-X
Mining areas
Geodetic monitoring
Open pit deformation
Amazon region

ABSTRACT

The Carajás mineral province encompasses the world's largest iron reserves with excavation carried out through open pit benching. Mining operations in the area have significant areas of rock mass movements and surface displacements that potentially lead to slope instabilities with risks to personnel, equipment and production. Instabilities can be expected due to deep excavations in rock masses of low geomechanical quality, blasting practices and heavy precipitation. In this paper, ground instabilities are monitored through an integrated SAR analysis based on a data-stack of 33 TerraSAR-X images. This approach was designed to monitor distinct displacement regimes, ranging from small to high deformation rates, and to map surface changes, based on variations of radar reflectivity. Results were compared with field information (total station/prisms, ground based radar, geological and geomechanical maps), and the approach showed to be effective for monitoring ground deformation in the region. Due to its capabilities (synoptic view, high accuracy, dense grid sampling), the complementary use of space-based SAR with field monitoring systems proved to be strategic for operational mining planning and risk assessment in this challenging environment.

1. Introduction and context

Iron accounts for 95% of the world's metal production in terms of weight, and Brazil is the second largest producer of iron ore (IBRAM, 2013). The Carajás mineral province (CMP) encompasses reserves of 18 billion tons with an average grade of 65.4% Fe content. The deposits encompass 39 bodies showing profiles with horizons, which correspond to progressively upward physico-chemical degradation from lateritic crust to clayey to earthy soil (Horbe and Costa, 2005). The entire mining operations are guided by an automated system that controls each step in the production process in real time via satellite.

Instabilities are common at this mining activity in the Carajás complex. Rock mass movements and surface deformations potentially lead to slope instabilities or wall failures due to the open pit mining operations. The collapse of a slope can cause risk to personnel and equipment, mining infrastructures, disrupting mine scheduling with an increase in production cost. In the study area, deep excavations in rock masses of low geomechanical quality, coupled with blasting practices and heavy precipitation contribute to instabilities. As a consequence, the open pit complex of Carajás, particularly N4E mine, considered the world's largest iron ore by volume removed and linear extension (more than 4 km), has presented multiple slope failure events. It is worth noting that small surface movements on a mine highwall may be a sign of instability. Thus, an effective prediction and management of ground deformations should be a key concern for the mining industry.

Most major open pit mines employ geotechnical teams to monitor movement, and review the ground stability data using monitoring systems. These systems can be divided into two categories: surveying and geotechnical techniques (Jaroz and Wanke, 2003). Surveying techniques are used to determine the absolute positions and positional

* Corresponding author at: INPE, Avenida dos Astronautas 1758, São José dos Campos CEP 12227-010, Brazil.
E-mail addresses: waldir@ltid.inpe.br (W.R. Paradella), alessandro.ferretti@treuropa.com (A. Ferretti), mura@dpi.inpe.br (J.C. Mura), davide.colombo@treuropa.com (D. Colombo), fabio@dpi.inpe.br (F.F. Gama), andrea.tamburini@treuropa.com (A. Tamburini), athos@ltid.inpe.br (A.R. Santos), fabrizio.novali@treuropa.com (F. Novali), galo@fct.unesp.br (M. Galo), paulo@fct.unesp.br (P.O. Camargo), arnaldoq@ufpa.br (A.Q. Silva), gsilva@dsr.inpe.br (G.G. Silva), aristotelina.silva@vale.com (A. Silva), leonardo.leopoldo@vale.com (L.L. Gomes).

http://dx.doi.org/10.1016/j.enggeo.2015.04.015

changes of any point on the surface and distinct instruments are utilized (total stations/prisms, robotic total stations, geometric leveling, GNSS-Global Navigation Satellite Systems, photogrammetric cameras, terrestrial LASER-Light Amplification by Stimulated Emission of Radiation scanning, etc.). Geotechnical techniques employ punctual instrumentation (crack measuring pins, extensometers, inclinometers, piezometers, etc.) to measure deformation over a relatively short measurement base. The main advantage of the conventional monitoring techniques is the high accuracy of measurements. However, these measurements are limited by complicated and costly instrumentation, high influence of field and weather conditions, discrete character of observations and high cost of frequent surveys.

A classification scheme of monitoring systems for open pit mines was recently presented. In this scheme (Vaziri et al., 2010), instruments were related to surface measurement techniques at discrete points (total stations/prisms, extensometers, etc.), and over areas based on scanning (ground based radar, LASER, etc.) and image-based techniques (photogrammetry). It is important to consider that systems that monitor displacements over large areas yield more information than systems designed for monitoring points, since the former can provide data about the spatial patterns of deformation. In Carajás, climatic conditions and mining activities (clouds, precipitation, dust cover) limit the use of aerial photogrammetry and laser scanning for operational monitoring of deformations. Lower cost instruments, such as total station/prism and extensometers, are normally used for primary monitoring, but once instability has been detected, the ground-based radar is the best monitoring alternative, particularly when visibility and accessibility cannot be guaranteed. Prisms and ground-based radar are important monitoring systems and are generally considered as complementary and provide important calibration. The prism-monitoring system provides a very cost-effective way of measuring 3D displacement and is used to get an overview of the movement in the pit, while ground-based radar focuses the view on a sector of the mine. Mining operations generally have variable geotechnical conditions and related distinct failure mechanisms. In large open-pit mines such as in Carajás, it is essential to use multiple monitoring systems to ensure a balanced slope risk strategy. Since the research encompasses significant areas of mining, with a demand of movement information, within and beyond the pit limits including waste piles, tailing ponds, dams, transport routes and processing facilities, the use of Differential Interferometric Synthetic Aperture Radar (DInSAR) for monitoring is justified, particularly due to the versatility of systematic all-weather data acquisition through satellite systems. The advantages of DInSAR over total station/prisms or ground-based radar are that measurements can be made without fieldwork and detailed motion information (millimeter scale) can be provided over large areas.

Although radar technology has been used for the last 50 years, only in the last decades the hardware–software capabilities provided the power for DInSAR processing. The first demonstration of satellite repeat-pass DInSAR to detect deformation was presented in the 1990's (Gabriel et al., 1989). Apart from cycle ambiguity problems, limitations due to temporal and geometrical decorrelations and atmospheric artifacts have limited the use on a fully operational basis of DInSAR based on single interferograms (Colesanti et al., 2003). In order to overcome these drawbacks, a new trend emerged with the advent of Advanced DInSAR (A-DInSAR) techniques, which are based on the processing of temporal series of SAR data to form time series of deformation. The Permanent Scatterer Technique (PSInSAR™), the first of a family of A-DInSAR algorithms, deals with the identification and monitoring of point-wise permanent scatterers (PS), pixels that exhibit stable amplitude and coherent phase throughout the whole dataset (Ferretti et al., 2000, 2001). PS are related to radar targets such as rocky outcrops, boulders, metallic structures and man-made objects, and are less present in non-urban areas and absent over heavily vegetated terrains. In order to overcome the limits of PSInSAR™, a new technique known as SqueeSAR™ was recently presented (Ferretti et al., 2011). This new algorithm extracts information from both PS and DS (distributed scatterers), significantly improving the spatial density of measurement points in non-urban areas.

In the mining industry, satellite DInSAR technologies are becoming more relevant for several reasons: they allow mining engineers to detect deformation at low cost, without having to install in-situ instruments. Displacement precision in the line of sight of the sensor (LoS) can be lower than 5 mm on individual measurements and information can be extracted over a dense grid of points, depending on the spatial resolution of the radar system. The data can provide a synoptic view of the deformation field affecting the area of interest, as well as its spatio-temporal evolution. Many examples were published related to underground mines (Crosetto et al., 2005; Colesanti et al., 2005; Herrera et al., 2007; Perski et al., 2009; Ng et al., 2010) with few papers to open pits (Wegmuller et al., 2007; Herrera et al., 2010; Hartwig et al., 2013). In a classical compendium on open pit slope design, A-DInSAR is presented as a monitoring tool more suitable for detecting ground subsidence and post closure movements rather than for slope monitoring (Hawley et al., 2009).

The complexity of the open pit mining in CMP makes DInSAR a challenging application for deformation monitoring. The main objective of this work is to show the potential of an integrated SAR analysis for mapping displacements within and around the large open pit iron mining complex of Carajás, providing long-term monitoring solutions for in-pit mining operations including waste piles and other surface assets without the need for ground instrumentation. To this end, a large set of X-band data acquired by the TerraSAR-X (TSX-1) satellite was examined and demonstrated, through the discussion covering distinct sectors of the Carajás complex, the capability to detect and analyze deformation phenomena for monitoring and predicting surface instabilities. The strategy is based on a combination of different SAR techniques to monitor (1) slow deformation (from millimeters up to centimeters per year) through SqueeSAR™ analyses, (2) fast deformations (up to few meters per year) using simple unwrapped interferograms and Speckle Tracking (ST) maps (based on the temporal series of amplitude radar images, where individual features can be tracked in time), and (3) surface changes using amplitude change detection (by comparing the backscatter of two images pre- and post-failure events). The results were compared, whenever possible, with information provided by Vale mining company, represented by field based measurements (total station/reflective prisms, ground based radar), geological and geomechanical maps. The research has shown that the Integrated SAR approach combined with geotechnical field techniques offers the best solution for monitoring purposes in this difficult terrain.

2. Study area

The CMP, located in the easternmost border of the Amazon region, is the most important Brazilian mineral province. Following the iron deposit discoveries in the 60's, other metalliferous deposits have been identified including manganese, alumina, nickel, tin, gold, platinum group elements and copper. The region is marked by mountainous terrains, characterized by hills and plateaus surrounded by southern and northern lowlands, deep chemical weathering which produces thick oxisols, totally covered by Ombrophilous Equatorial forest (Paradella et al., 1994).

A remarkable structural feature in the region is an open synclinorium, about 200 km long and 40 km wide, aligned WNW–ESE. Outcrops of iron formations form high, normally bare, laterite-capped plateaus, which stand above the equatorial forest. The northern limb of this synclinorium is marked by an irregular line of nine plateaus (collectively called Serra Norte), while the southern limb forms another such line (Serra Sul). The mining activities on Serra Norte are concentrated on two iron orebodies (N4 and N5) and were started by 1984 with the N4E mine. Now spanning five simultaneous open-pit mine

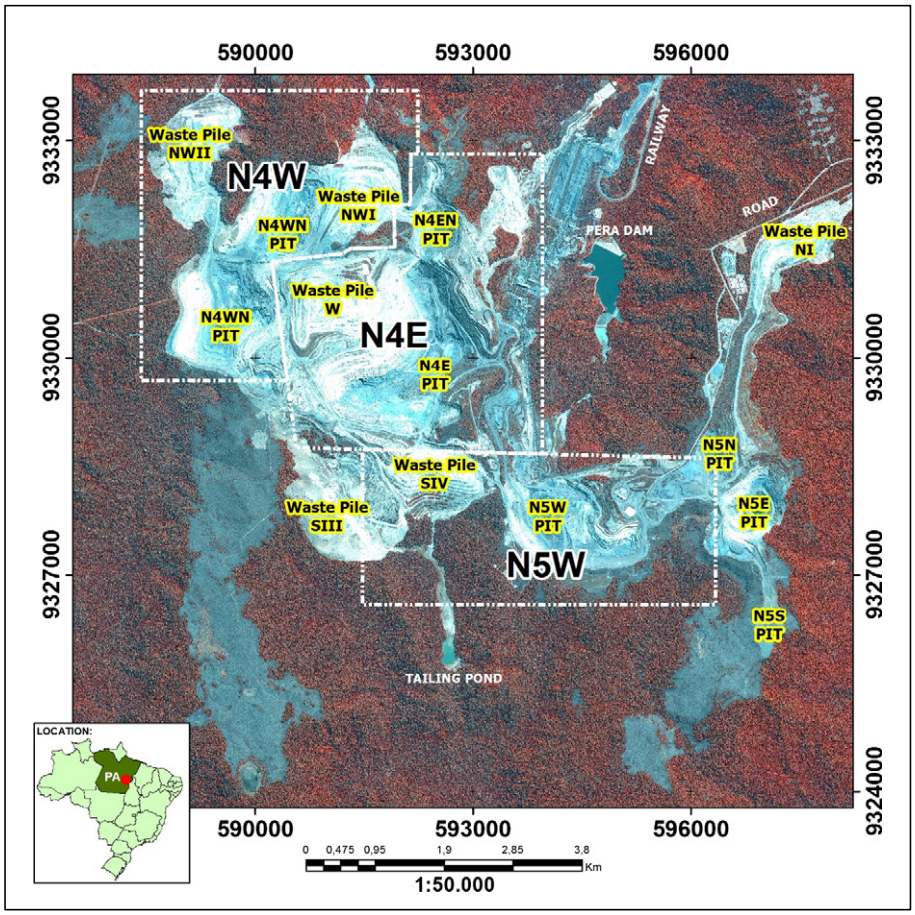

Fig. 1. GeoEye-1 color composite image (bands 4, 2, 3 as RGB) acquired on the 1st of July 2012 showing the mines and related structures, and location of the study area in the Amazon region (Pará state, Brazil).

operations (Fig. 1), Carajás complex presented a strong performance in the second quarter of 2014 reaching an iron ore production of 29.3 Mt.

2.1. Regional geology

The CMP is tectonically included in the Archean Central Amazonian Province (Tassinari and Macambira, 2004) in the southern part of the Amazonian Craton. Its northern domain corresponds to the Carajás rift affected by the E–W trending Archean Itacaiúnas Shear Belt (ISB). The ISB (Fig. 2) is characterized by two lithostructural domains: a set of imbricated ductile oblique thrusts on the southern sector and two strike-slip systems (Carajás and Cinzento) on the northern sector (Holdsworth and Pinheiro, 2000; Veneziani et al., 2004). The Carajás strike-slip system is the largest fault system recognized within the ISB. A reasonable amount of SAR data has been evaluated in the CMP for geological mapping (Paradella et al., 1997), topographic mapping (Oliveira et al., 2011), and discrimination of iron-mineralized laterites (Silva et al., 2009).

2.2. N4E iron mine

2.2.1. Geological, lithostructural and geotechnical setting

The N4E iron mine was chosen for this paper due to two characteristics: it is the world's largest open pit iron mine and has presented a record of relevant number of instabilities. The mine lies on the NE branch of the N4 plateau, and is a massive excavation (525 ha) on an orebody with 350 m thick, 4.1 km long, 300 m wide, 425 m depth and with 15-meter-high benches. The reserves (proven + probable) for December 2012 were 345.1 tons with 66.4% of iron concentration. The deposit is related to metavolcanic and metasedimentary rocks of the Grão-Para Group subdivided into two units: the volcanic rocks of the Parauapebas Formation (Meireles et al., 1984) and the ironstones of the Carajás Formation (Beisiegel et al., 1973). The ironstones of the Carajás Formation are represented by jaspilites and iron ores, intruded by dikes and mafic sills. All the rocks were affected by low metamorphic grade.

The most detailed available account of the geological and geomechanical information for the N4E open-cast pit was originally presented by Sá (2010) and further complemented by work conducted by BVP (2011). Surface outcrop mapping at 1: 2000 scale was performed with rock classification based on mining nomenclature, characterization of structural and geomechanical parameters, with strength tests for rock units and back analysis of slope failures. According to BVP (2011), the mine is composed by rock masses defining heterogeneous and anisotropic products with different responses to shear strength. The geological and geomechanical maps are presented in Fig. 3. Mafics are country rocks of the iron ore, which are normally covered by lateritic duricrusts. Based on geotechnical parameters, the mining nomenclatures for mafics are: unweathered mafic, weathered mafic with inferior resistance, weathered mafic with medium resistance, weathered mafic with superior resistance and semi-weathered mafic. The ironstones are classified based on physical-chemical parameters in jaspelite, soft hematite (laminated and powdery hematite), hard hematite and low content iron ore. Depending on the intensity of the foliations, soft hematite can be classified as strongly laminated, weak/moderate laminated and powdery. Hard hematite and low content ore crop out as small lenses and small body, respectively. Basic dykes and sills are emplaced into these units that are covered by layered iron duricrusts and lateritic soils.

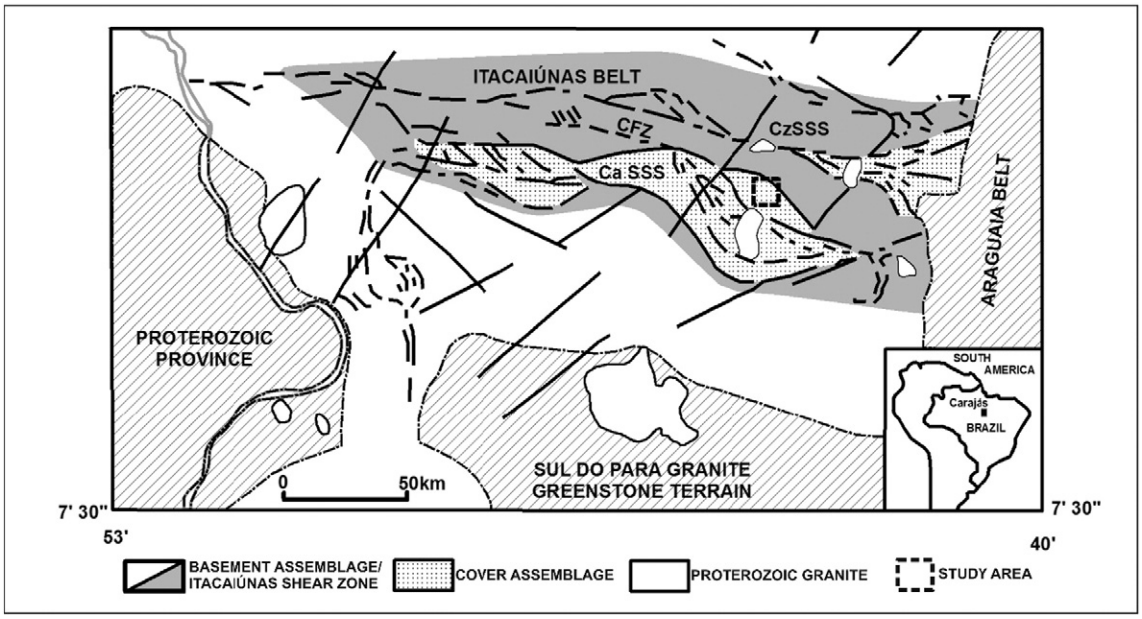

Fig. 2. Regional structural map of the ISB adapted from Holdsworth and Pinheiro (2000). Legend: CFZ = Carajás Fault Zone, CaSSS = Carajás Strike-Slip System, CzSSS = Cinzento Strike-Slip System.

The main structures from the detailed mapping are: (a) banding or foliations showing shear evidences and dipping to W, (b) ductile shear surfaces with NE–SW trending direction, (c) joint systems with sub-vertical trends oriented to NNE–SSW and to NW–SE, and (d) strike-slip fault systems showing dextral and sinistral kinematics, with trends oriented to NW–SE and to NE–SW, dipping to NE and SW. The results of

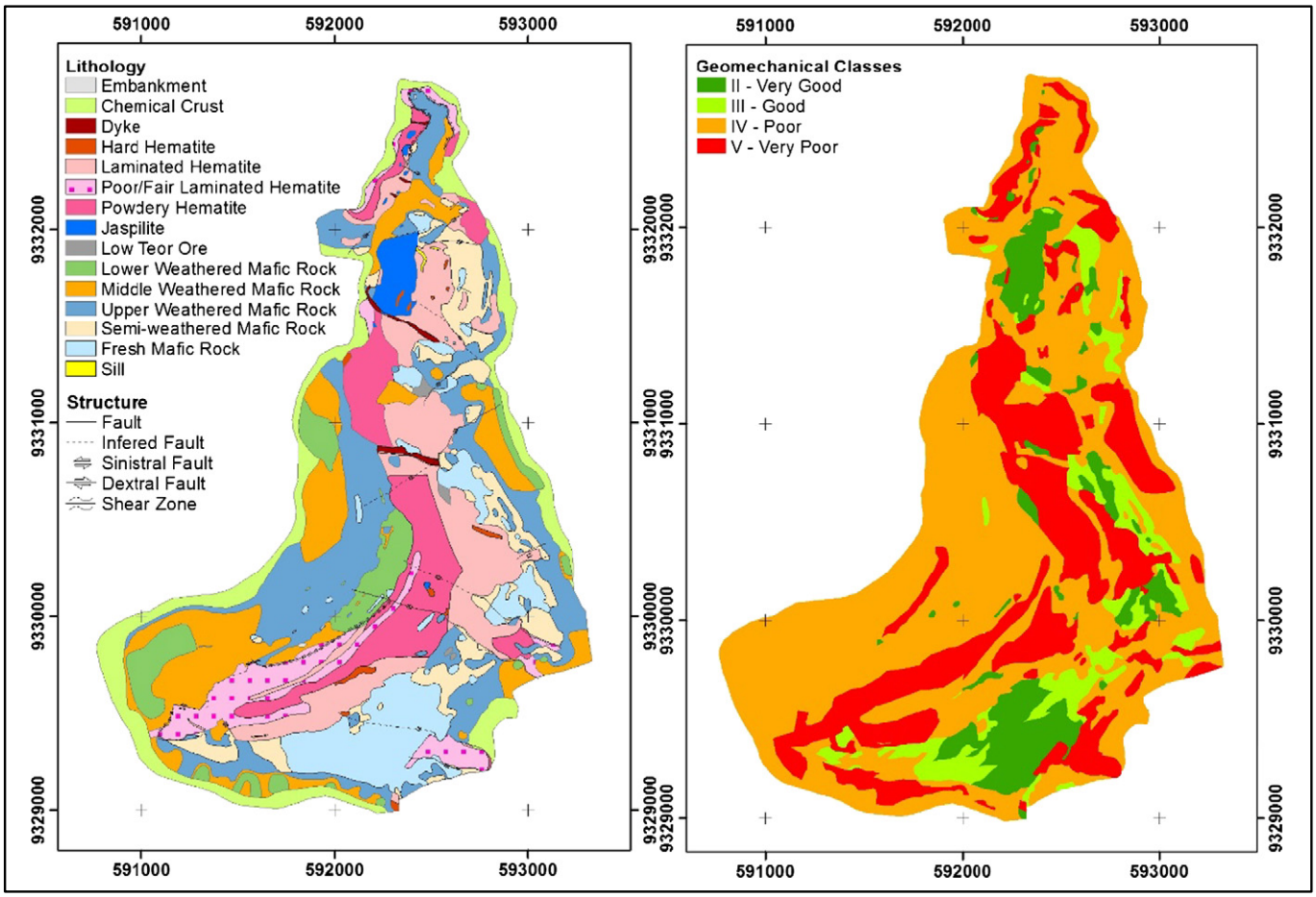

Fig. 3. Geological and geomechanical maps of N4E mine.
Source: BVP (2011).

strength tests and back analysis of slope failures (Sá, 2010) indicated that the main lithotypes, particularly soft hematite and weathered mafics, exhibited an overall poor strength ranking classification according to ISRM (1981), and were classified as soil (compressive strength of rocks <0.25 MPa). In addition, the rock masses were classified based on RMR (Rock Mass Rating) parameters (Bieniawski, 1989) with results presented in Table 1.

2.2.2. Slope instabilities and monitoring system

A history of instabilities in the N4E slopes has been compiled for the period of the investigation (Vale, 2012, 2013). The events are related to benches (walls and floor) on two sectors of the pit: western flank and central pit. The events showed a variation of intensity ranging from small movements, settlements, presence of tension cracks, rock falls, failures and even collapses. The slope monitoring system in the mine includes visual inspections to detect the onset of instabilities and field measurements with total station/prisms and SSR—Slope Stability Radar (a ground-based radar built by GroundProbe Pty Ltd). A summary of the characteristics of the slope instabilities is presented in Table 2.

3. Satellite dataset

A stack with 33 TSX-1 StripMap images was planned for the investigation. However, conflicts in acquisition programming of the satellite caused four interruptions in the coverage in 2012 (Dec 31) and 2013 (Feb 13, Feb 24, Mar 07). The Single Look Complex images were acquired under ascending passes (look azimuth ~ 80°), incidence angle range of 39.89°–42.21°, spatial resolution of 1.7 m × 3.49 m (range × azimuth), pixel spacing of 1.36 × 1.90 m (range × azimuth). Unfortunately descending passes were not available that would permit interferometric measurement using both viewing to provide quasi vertical and east–west components of the displacement (Rucci et al., 2013). The minimum and maximum perpendicular baselines were 7.18 m and 487.65 m, respectively. The master image for the interferometric processing was acquired on July 5, 2012 and the maximum temporal offset was 319 days.

The key-element in any interferometric analysis is the phase value of radar image pixel. Phase values of a single SAR image are related to the sensor-to-target distance and therefore depend on the local topography. A high-resolution GeoEye-1 DEM was used in the interferometric process and for the production of orthoimages (panchromatic and multispectral) for field validation. In-track GeoEye-1 stereo pairs were acquired on July 1, 2012. The first scene was collected with azimuth and elevation angles of 29.4° and 82.4°, whereas the second scene was acquired with azimuth and elevation angles of 187.42° and 62.20°. The images were provided with 0.5 m spatial resolution and RPCs (Rational Polynomial Coefficients). In order to maximize the mapping of structures, a geological interpretation of a RADARSAT-2 Ultra-fine (RST-2 UF) stereo-pair was also carried out. The RST-2 images were acquired in 2009 (Jul 09, Jul 23), on descending passes (look-azimuth around 280°), and correspond to beam modes UF5 and UF21, with spatial resolution of 3.38 × 2.8 m (UF5) and 2.44 × 2.80 m (UF21).

Table 1
Summary of the geotechnical RMR parameters of rock class.

Lithotype	Class
Jaspellite	II (very good rock)
Hard hematite	II (very good rock)
Fresh mafic	II (very good rock)
Semi-weathered mafic	III (good rock)
Soft-hematite	V (very poor rock)/IV (poor rock)
Weathered-mafic	V (very poor rock)
Low content ore	V (very poor rock)

Table 2
Instabilities in the N4E during the investigation.
Sources: Vale (2012, 2013).

Event	Location	Characteristics
Aug 27 up to Sept 10/2012	Western flank	Presence of settlements (1.5 m of vertical offset) and tension cracks. Variations of progressive and regressive deformations in bench faces leading to small ruptures. Loose masses (soil, debris) fall from the slope walls (rockfalls). Maximum detected deformation measured by SSR was 3272 mm.
Feb 27 up to Mar 11/2013	Central pit	Several progressing deformation episodes characterized by strong movements in pit walls, collapses of slopes, presence of fractures on the surface and talus mass movements. Maximum accumulated deformation measured by SSR was 1103.14 mm.

4. General methodology

Depending on the purpose of the analysis (extent of the area, required frequency of temporal updates, spatial density of measurement points, displacement rates, etc.), different SAR processing algorithms can be applied for monitoring mining areas. In the study area, instabilities have showed a variation of intensity ranging from small to strong movements over the pit slopes and settlements related to waste piles. In addition, intense variations of SAR responses are characteristics of this rapidly changing environment.

In this investigation, we applied an integrated SAR analysis aimed at extracting as much information as possible about the phenomena affecting the area of interest. Three complementary approaches to measure slow (few millimeters up to some centimeters per year) and fast ground deformations (up to few meters per year) were addressed. In addition, change detection based on the comparison of two or more amplitude SAR images was also highlighted as the first step for characterizing the evolution of the area. The synergistic use of different techniques allows a better understanding of the phenomena affecting the area of interest and improves the reliability of the SAR analysis. The proposed methodology relies on the combination of distinct source of information provided by the integrated SAR analysis with visual interpretation of RST-2 UF stereo-pair and field geological and geomechanical data. In order to remove the topography phase in the interferometric processing an external GeoEye-1 derived DEM was used. The main steps of the proposed workflow are discussed in the following subsections.

4.1. GeoEye-1 DEM generation

The Rational Function Model (RFM) has been one of the most common geometric modeling methods in order to extract the DEM from stereo data (Tao and Hu, 2001). This method uses the RPCs provided with the satellite metadata to compute the model, and a panchromatic DEM was produced at 2 m spacing using one ground control point (GCP). The DEM elevation values were compared to seven accurate vertical check points, and root-mean-square-error and maximum errors of 1.2 m and 1.6 m, were obtained (Paradella and Cheng, 2013). Panchromatic and multispectral orthoimages were also produced using as input the DEM and GCPs with a root-mean-square-error around 1 m for planimetry (X,Y).

4.2. Geological photointerpretation using RADARSAT-2 stereo-pair

Previous research in CMP with radar stereo pairs showed that stereo viewing has provided valuable information in the definition of high and low-angle dipping strata, lithological contacts and general discontinuities (Santos et al., 1999). Thus, RST-2 UF pair was analyzed using the graphical interface of viewing and digital enhancements available in the OrthoEngine 3D Stereo package (PCI Geomatics software). The visual interpretation consisted in the detection and analysis of linear

features with lithological–structural significance, expressed as negative ruptures (lithological contacts), positive and negative linear features (faults, dikes, etc.), symmetric-asymmetric patterns (attitude of planar structures) and array (kinematic and/or complexity of structures).

4.3. SAR processing steps

As already mentioned, an integrated SAR analysis combining four different SAR techniques has been used for processing multi-temporal data acquired by TSX-1 over the area.

4.3.1. Change detection maps

Change detection maps are based on the comparison of two or more amplitude SAR images (Scheuchl et al., 2009) and are the first step for characterizing the evolution of the study area. Although not providing displacement measurements, change detection maps can highlight areas affected by mining operations or severe deformation. Amplitude values of a radar image are related to the amount of electromagnetic energy backscattered toward the satellite by targets on ground. Time lapse analysis of amplitude radar images provides a powerful tool for highlighting possible changes occurring within the area of interest, independently of sun illumination and cloud coverage (Rignot and van Zyl, 1993). Reflectivity changes can be induced by many factors, such as: morphological changes, soil moisture variations, vegetation growth and anthropogenic causes. During the monitoring of mining activities, it is usually quite easy to identify the cause of a certain change, by comparing change detection maps with the schedule of the operations.

4.3.2. Deformation maps from unwrapped interferograms

The easiest way to detect small variations in the topography of an area by means of satellite radar data is the generation of an

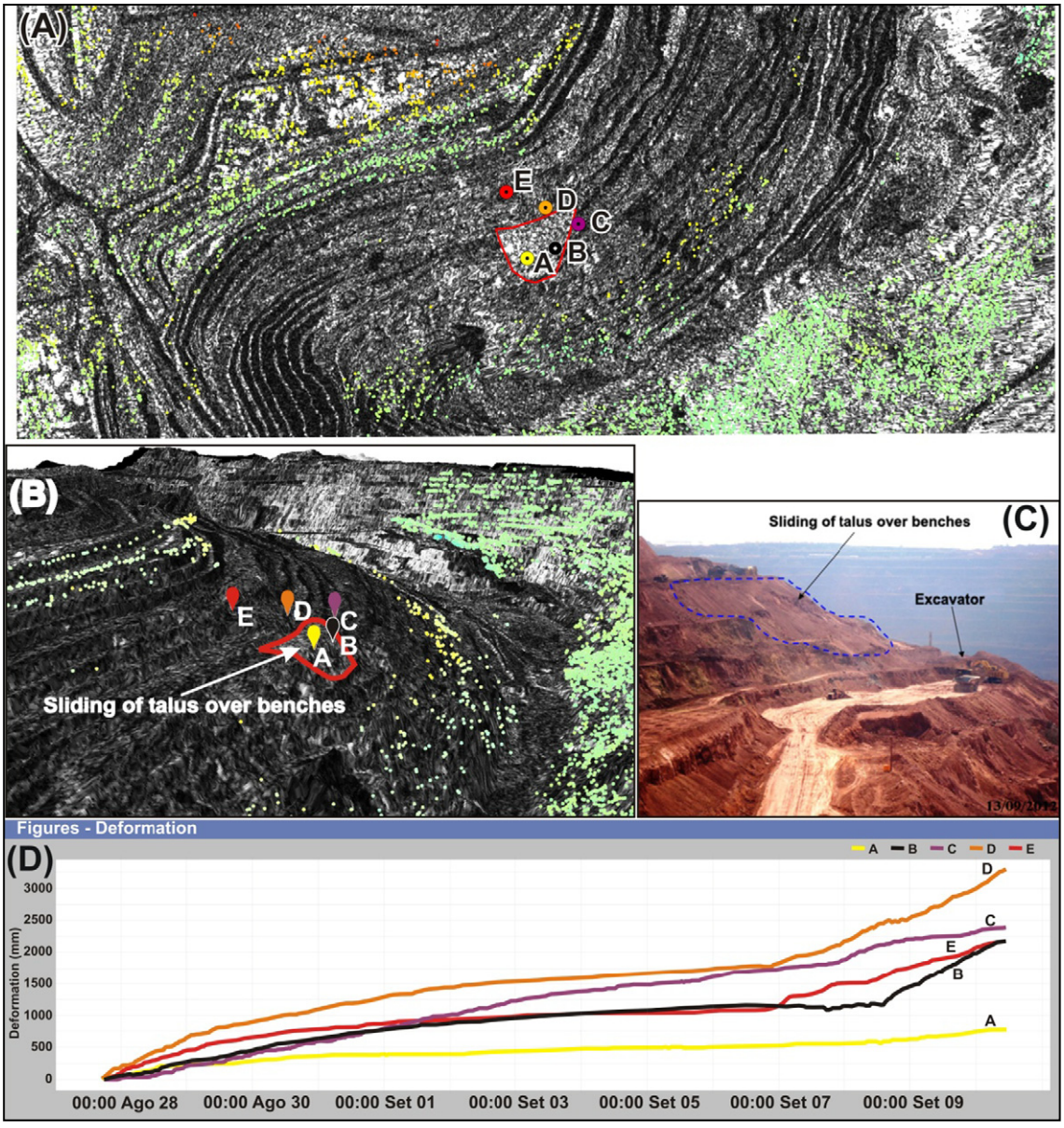

Fig. 4. (A) TSX-1 image of the Western flank of N4E mine, acquired on Sept 12, 2012, showing an area of a rockslide (red triangle with high backscattering response) as detected by amplitude change detection and locations of bench walls (letters A, B, C, D, E) that were field monitored with SSR. The overall absence of SqueeSAR™ PS/DS nearby was due to a loss of SAR coherence, (B) 3D perspective of the same SAR image with indication of rockslide area and location of SSR measurements, (C) field picture taken on Sept 9, 2012 of the rockslide event, (D) SSR deformation profiles related to bench walls.

interferogram using two SAR images acquired at different times (Gabriel et al., 1989). Phase values are related to the sensor-to-target distance, therefore phase changes recorded by a SAR interferogram can highlight possible range variations. Phase values of a SAR interferogram are known modulo-2π. In order to estimate a displacement map, phase data have to be unwrapped, by applying proper phase unwrapping algorithms. The reliability of any unwrapping procedure, as well as the impact of atmospheric effects and possible other noise sources on the interferogram, can be assessed only by using more than one data pair acquired over the area (Ferretti et al., 2007). The maximum displacement rate that can be detected by means of a single SAR interferogram depends, apart from the noise level in the interferogram, on the operating frequency of the radar system and the gradient of the displacement field (the smoother the field, the easier the unwrapping). In general, the shorter the wavelength (and so the higher the frequency), the higher the sensitivity of the interferometer to any displacement, but the more likely a phase unwrapping error. Although it is very difficult to provide some ball-park figures, in mining areas, with a SAR sensor operating at X-band and a 11-day repeat cycle, it is difficult to track displacement phenomena generating a range change of more than a few mm/day. Unwrapped interferograms may not be the tool for millimetric displacement measurements, although it is still useful in providing qualitative information over unstable areas, mainly through a synoptic view of displacement distribution over small time intervals (small temporal baseline). This technique is used to extract ground deformation data when an insufficient number of SAR images are available over an area of interest to perform a full SqueeSAR™ analysis.

4.3.3. SqueeSAR™

The PSInSAR™ technique (Ferretti et al., 2001), developed in the late 1990's at Politecnico di Milano (POLIMI), was the first of the so-called "advanced InSAR algorithms" aiming at overcoming the difficulties related to conventional InSAR analyses, namely: atmospheric artifacts and temporal decorrelation. The basic idea is to compare many SAR images (rather than just two, as in conventional InSAR) and focus the analysis on a sub-set of image pixels exhibiting a very coherent radar signature in time, the so-called Permanent Scatterers (PS). PS allow the implementation of powerful filtering procedures to estimate and remove atmospheric noise. PS results can be accurately geocoded and integrated with other prior information. The SqueeSAR™ technique represents the second generation PSInSAR™ approach allowing one to obtain a significant increase of measurement points over non-urban areas by exploiting two families of ground measurement points:

- Permanent Scatterers (PS): point-wise radar targets characterized by high reflectivity values, generating very bright pixels in the SAR scene, usually corresponding to man-made objects, pylons, penstocks, outcrops, boulders, etc.
- Distributed Scatterers (DS): radar targets usually corresponding to many adjacent pixels in the SAR image, all exhibiting a very similar radar signature and where temporal decorrelation phenomena, though present, still allow the retrieval of displacement data. These scatterers usually correspond to rocky areas, detritus, non-vegetated areas, etc.

Whatever the type of measurement point (MP) identified by the algorithm, provided that enough SAR images are available over the area of interest, the following information can be retrieved: geographic coordinates of the MP (latitude, longitude, elevation), average displacement rate (in mm/year) and time-series of displacement values (in mm) with respect to the first SAR acquisition. All displacement measurements associated with a MP are the projection, along the satellite Line of Sight (LoS), of the 3D displacement vector affecting the target. These are differential measurements with respect to a reference point selected within the area of interest, time referenced to the acquisition date of the first image. Therefore, displacement data provided for each MP are relative, not absolute, data. The accuracy of measurements depends on many parameters such as number of SAR images, spatial distribution of PS/DS, climatic conditions, distance from the reference point and quality of PS/DS within the area of interest. The standard deviation of the velocity values estimated with respect to the reference point is a very important parameter for precision assessment and can be estimated directly from the data available. Typically, using datasets of more than 20–30 satellite images, it is not uncommon to obtain precision better than 1 mm/year on displacement rates, while error-bars on individual measurements are usually lower than 5 mm. More details on precision and accuracy of the measurements can be found in Ferretti (2014).

MPs can be seen as a 'natural' ground network of radar benchmarks (similar to a GNSS network) that can be used for monitoring both the displacement of individual structures and the evolution of large areas. It should be noted that MP density is usually much higher than the density of benchmarks available in conventional geodetic networks and does not require any installation of field instruments or other field work (a key feature for mining applications) and fast algorithms are available to update the information quickly and reliably. A further advantage of SAR interferometry with respect to conventional geodetic techniques is the possibility to exploit radar data acquired in the past (available in satellite archives) to quickly estimate the dynamics of an area of interest where no instrumentation has been installed. Finally, the introduction of new X-band SAR satellites, characterized by higher sensitivity to surface deformation (compared to previous available sensors operating at C-band), higher spatial

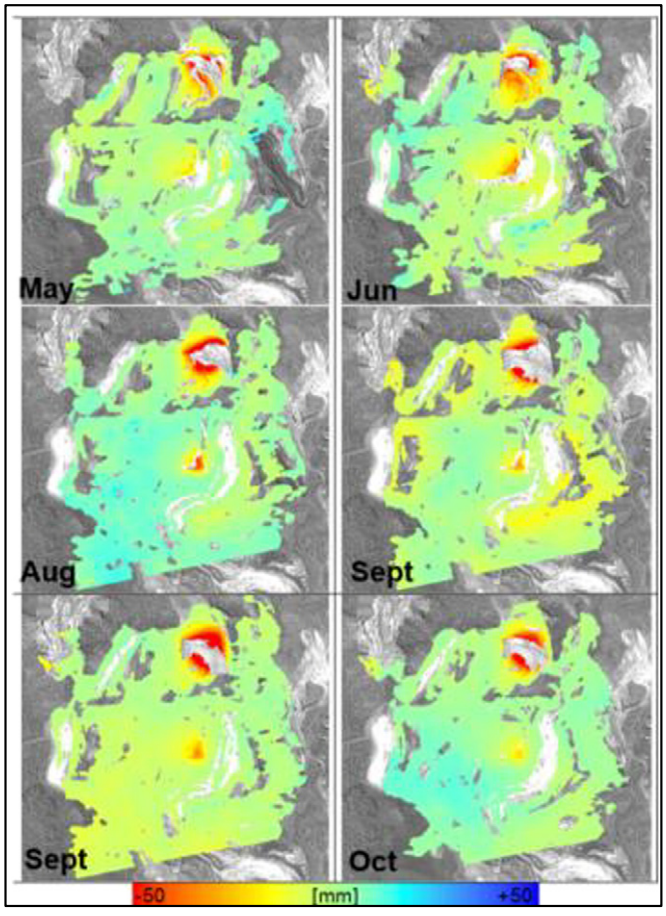

Fig. 5. Interferograms covering May–October 2012: strong deformations related mainly to NW-I waste pile settlements.

resolution (down to 1 m), as well as better temporal frequency of acquisition (down to a few days, rather than a monthly update), has further increased the quality of this kind of measurements and the impact on many applications.

4.3.4. Speckle Tracking (ST)

ST is a variant of feature tracking, which is based on the detection of movement of features identifiable in a time series of amplitude images. This kind of analysis makes it possible to obtain 2D displacement measurements from SAR imagery, in range and azimuth direction. Feature tracking has been extensively applied to the processing of optical image pairs in order to measure surface displacements of glaciers (Kääb, 2005). ST algorithms applied to SAR images do not require the identification of special features over the area of interest, but exploit the correlation of the speckle pattern between SAR image pairs, a phenomenon present in all coherent measurement systems. ST algorithms developed by TRE operate on a multi-image dataset, providing displacement time series, both in range and azimuth direction, for all areas exhibiting a consistent radar return over time (Raspini et al., 2014). The precision achievable with ST is not comparable with algorithms based on phase information and range and azimuth variations can be estimated with error bars that typically exceed 2–3 cm. Nevertheless, ST can be successfully applied in areas characterized by high displacement rates, up to tens of meters per year, which would appear as incoherent in any SAR interferogram. It should be noted that both amplitude and phase information are used in this integrated approach to monitor mining operations; doing so, both small (mm level) and large (even a few m) displacement values can be detected and monitored. The synergistic use of different techniques allows a better understanding of the phenomena affecting the area of interest and improves the reliability of the SAR analysis.

5. Results and discussions

5.1. Change detection maps

In a rapidly changing environment, as an open pit mining, monitoring change detection between two dates can be of utmost importance for several reasons (hazard management, map update, site monitoring, etc.). Change detection approach was also applied in the detection of slope ruptures in the Western flank. As previously mentioned (Table 2), SSR was used to monitor slope instabilities in this sector during the period of 27/Aug–10/Sept, 2012. The metric scale of deformation that was measured by SSR and field evidences (settlements, tension cracks on access ramps, sliding of talus over benches) recommended the usage of this approach to map areas affected by deformation ("*a posteriori detection*"). Fig. 4 shows a TSX-1 image acquired on Sept 12, 2012, a projected sliding area on a 3D perspective using this same SAR image, a field picture taken on Sept, 09, 2102 of rockslide event, locations and displacement time series of 5 control points monitored with SSR. The whither area (triangle) in the TSX-1 image (Fig. 4A, B) is interpreted as a rougher surface for the X-band signal, implying a higher

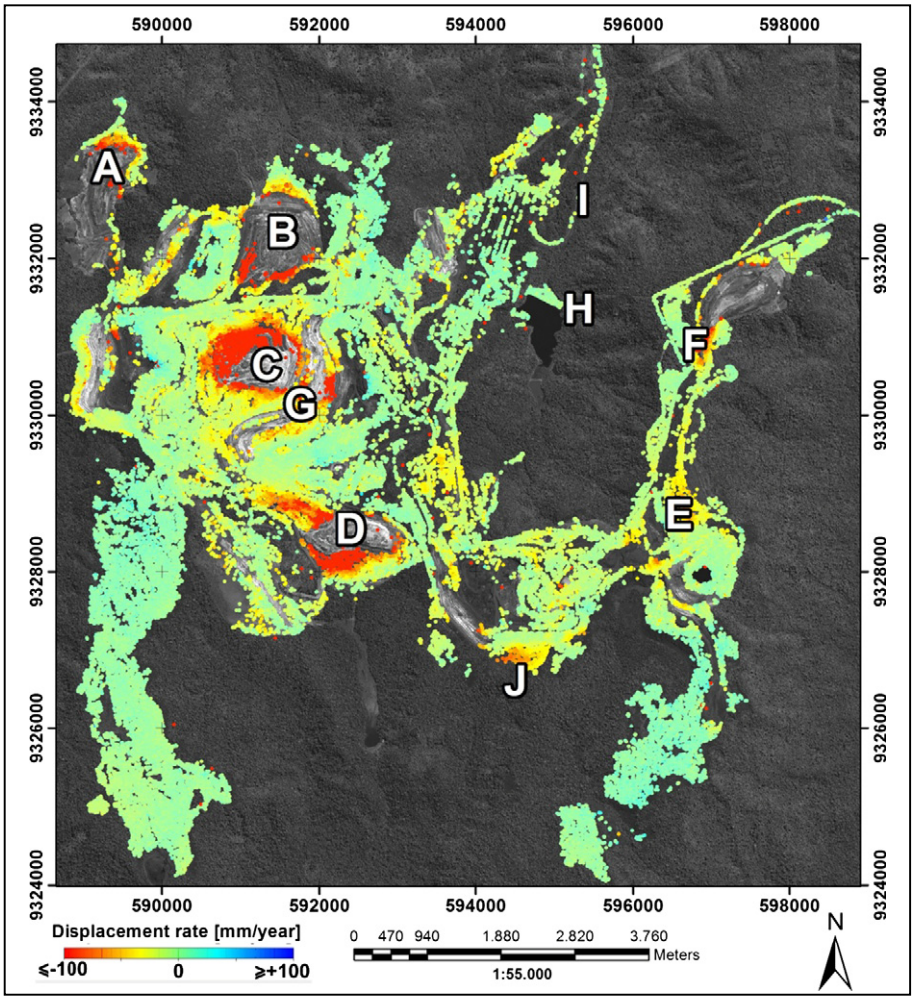

Fig. 6. MPs identified with the SqueeSAR™ analysis using the first 14 TSX-1 images, visualized by the average LoS velocity (mm/year) on the panchromatic GeoEye scene. MPs identified in this dataset all exhibit phase coherence values exceeding 0.85.

backscattered return induced by rockslides. The overall absence of SqueeSAR™ MPs (green/yellow dots) nearby was due to a loss of SAR coherence. Since the detection is less sensitive to subtle changes, but is robust to track surface changes based on backscatter differences, it still provides valuable information for remediation planning and risk assessments. Unfortunately, due to the failures of TSX-1 acquisitions, it was not possible to track evidences of slope ruptures that occurred in the Central pit area.

5.2. Unwrapped interferogram map

As already mentioned, the easiest way to detect small variations in the topography of an area by means of satellite radar data is the generation of an interferogram using two SAR images acquired at different times (Ferretti et al., 2007). In Fig. 5, six TSX-1 interferograms using images acquired 11 days apart are reported.

In general, the spatial coverage of points where coherence values are high enough to allow phase unwrapping of the phase values is better than what can be obtained with A-DInSAR techniques (such as SqueeSAR™), since no constraint is considered on the temporal coherence of the measurement points. However, deformation maps generated using just two SAR images are affected by atmospheric disturbances and possible DEM errors. In fact, only in a multi-interferogram framework, it is possible to discriminate between different phase contributions. In any case, short temporal baseline interferograms can be extremely valuable to detect abrupt changes in surface topography or the onset of sliding phenomena. Although this technique may not be the tool for accurate displacement measurements, it is still useful in identifying footprints of progressing movement.

5.3. SqueeSAR™ analysis

The processing was conducted in two stages covering the first 14 TSX-1 images, related to the dry season (23/Mar–10/Aug, 2012), and a final processing with all 33 TSX-1 images (23/Mar, 2012–20/Apr, 2013). PS and DS were detected and displacement rates expressed by average velocities computed with millimeter precision. Positive values correspond to motion toward the satellite; negative values correspond to motion away from the satellite (mm/year). For each MP, the (mean) annual LoS velocity and the displacement temporal series were calculated relative to a reference corner reflector on a stable area (location UTM 22 592250.772E 9332333.916N). SqueeSAR™ measurements are differential with respect to the reference point and their dispersion, expressed by the standard deviation of the estimated average displacement rates, increases with the distance to the reference point. It should be pointed out that the precision of the estimated displacement rate is affected by the number of the processed images and by the time period spanned by the dataset: the longer the time span, the higher the quality of the estimation.

The SqueeSAR™ analysis performed with the first 14 images has allowed the identification of 123,955 MPs with an average density of about 800 MPs/km^2 (Fig. 6). All MPs had phase coherence values (a measure of the goodness of fit of the model to the observations) higher than 0.85, with a standard deviation of displacement data typically lower than 2–3 mm. The number and distribution of MPs provided a unique view of the ongoing deformative processes in the Carajás complex. The map of the deformation rate shows that most of the iron mining complex was stable during the time span of the TSX-1 acquisitions (green-bluish regions). The highest deformation rates of the processing (yellow-reddish regions) were detected over the waste dumps (letters A, B, C, D, E, F), and some pit slopes (G), and a small pond (J). For the

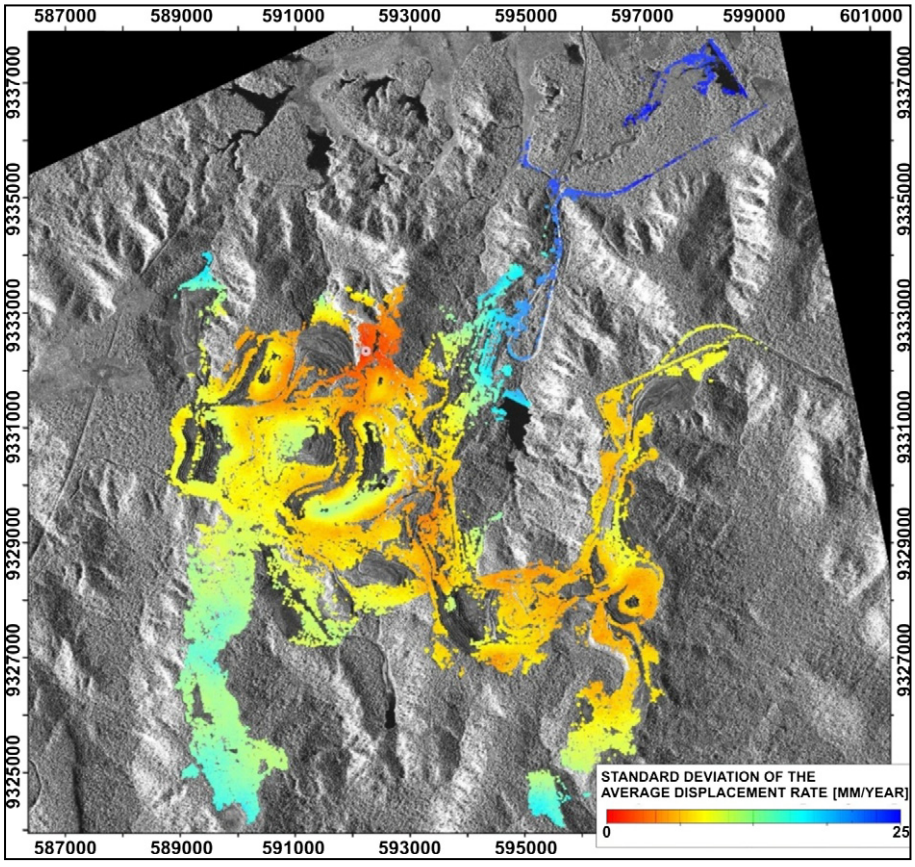

Fig. 7. Standard deviation map of the average displacement rates. Red areas correspond to low standard deviation values (1 mm/year), while blue points have higher dispersion values up to 25 mm/year.

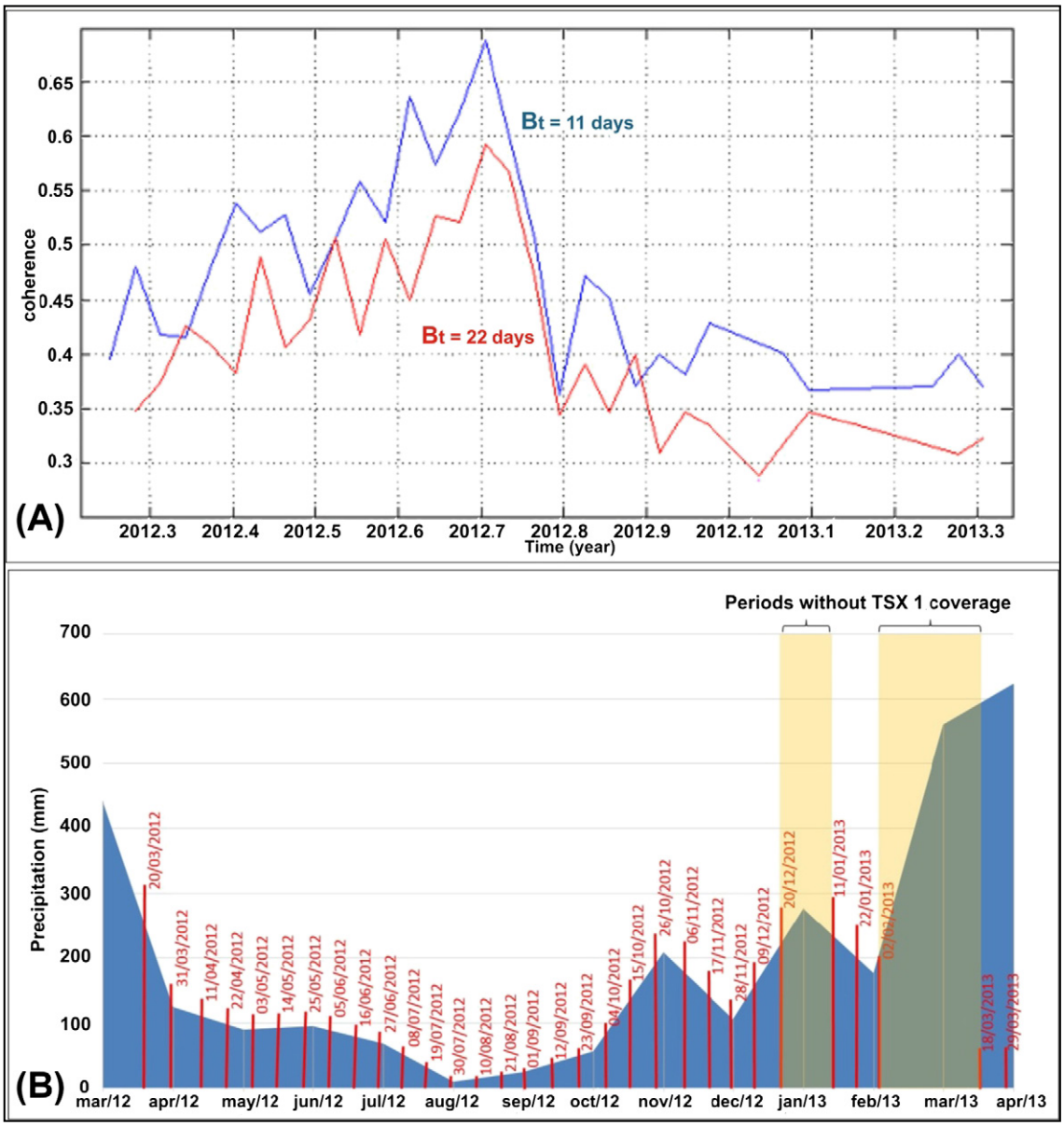

Fig. 8. (A) Coherence of interferograms for N4E mine from 20/March 2012 to 20/April 2013, computed with temporal baselines of 11 days (blue) and 22 days (red). (B) Corresponding precipitation values (blue color) and dates of the images acquisitions (red columns).

main infrastructure mining (dam, railway) the values indicated stability (H, I). High values of standard deviation of the estimated displacement rates were obtained for this first processing due to the use of a relative small number of images and short monitoring period (Fig. 7).

A coherence analysis of interferograms was undertaken for the whole time span over the N4E mine (Fig. 8A). The analysis was carried out for interferograms with Bt = 11 days (blue line) and with Bt = 22 days (red line), selecting only coherent areas, and highlights an evident loss of coherence with definition of two periods with distinct behaviors (Mar–Aug 2012 and Aug 2012–Apr 2013). Fig. 8B shows the precipitation values for the same periods. The comparison of both graphs clearly indicates that the loss of coherence is mainly caused by the rainfall variation, probably coupled with a rapidly changing environment induced by mining operations. As a consequence, when the stack of 33 images is processed, the detected MPs presented lower coherence values than those identified using images from the dry period only, due to the inclusion of low-coherence images. However, both deformation maps (Figs. 6, 9) revealed the same spatial patterns of displacements, and clearly highlight the important role that SqueeSAR™ technique could play in mining planning and risk assessment.

Under an ArcGIS environment, SqueeSAR™ results and raster thematic information (geological/geomechanical maps) were geocoded and superimposed on the panchromatic GeoEye orthoimage in order to explore spatial relationships. The SqueeSAR™ analysis with the first 14 TSX-1 dataset covering N4E mine let to the identification of 19,656 MPs (Fig. 10), while a slightly lower amount of MPs were detected (19,440) for the same area using all 33 images.

The highest SqueeSAR™ accumulated displacements and deformation rates provided by the A-DInSAR processing for the dry season (Fig. 10) were related to settlements of two major waste dumps, W pile (−185.85 mm and −474.6 mm/year, letter A,) and NW-1 pile (−165.48 mm and −420.9 mm/year, letter B). The rate of settlement of waste dumps is a controversial issue in the literature, since it depends on several parameters (dump height, dump type, loading rate, type of material, dump construction time, etc.), with large variations of

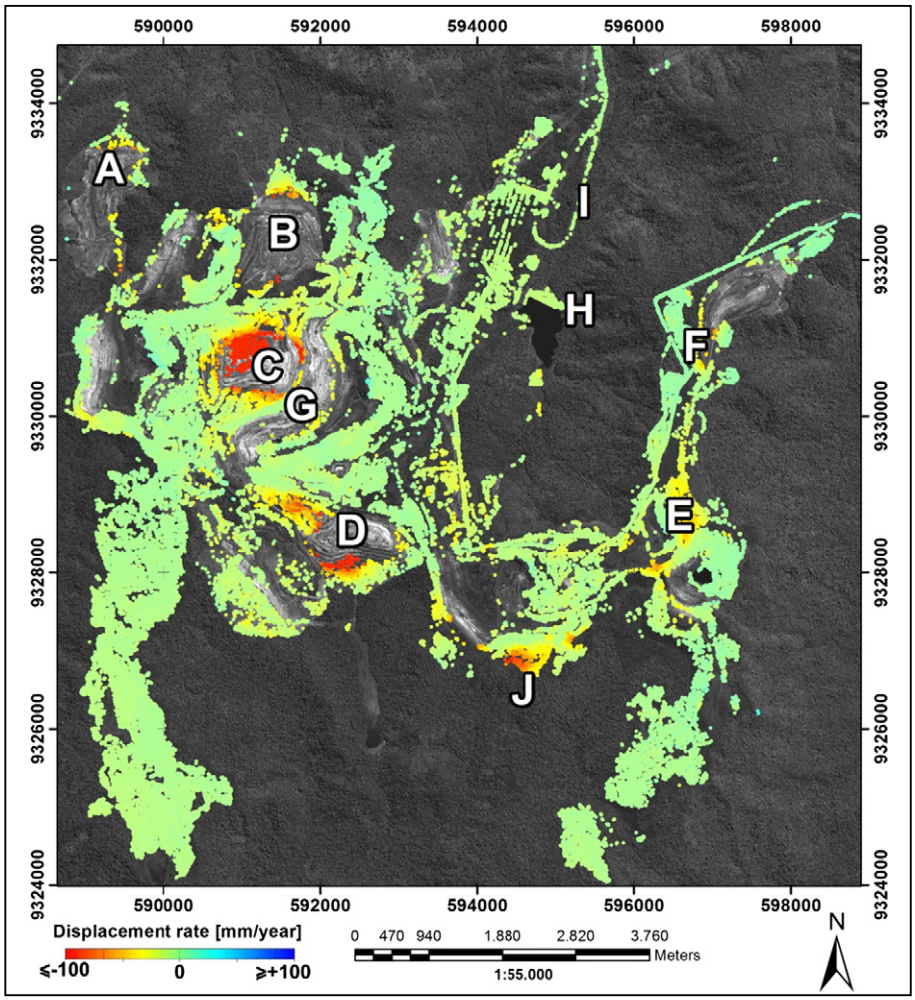

Fig. 9. MPs identified with the SqueeSAR™ analysis visualized by the average LoS velocity using the 33 TSX-1 images, from March 2012 to April 2013, on the panchromatic GeoEye scene (letters discussed in the text). MPs identified in this data-set exhibit phase coherence values exceeding 0.76.

settlements (0.3 up to 20%) regarding the waste dump height being reported (Orman et al., 2011), but in general, vertical settlements of few meters are normally expected.

Due to the overall absence of MPs for the NW-1 pile, it is concluded that this area has suffered significant surface changes, generating low coherence values. This aspect will be discussed later when dealing with ST analysis. However, it is important to mention that for both piles, displacement with positive value expressing motion toward the satellite characterized by bulging at the dump toe indicative of pile instabilities was not detected. Lower deformation rates corresponding to LoS range lengthening (possibly related to subsidence) were detected along two almost parallel belts of cut slopes on the western flank related to letters C (maximum accumulated displacements of −81.92 mm, deformation rates of −205.7 mm/year) and D (maximum accumulated displacements of −75.31 mm, displacement rates of −193.9 mm/year). This probable subsidence can be attributed to accommodation of upper weathered mafic rocks with poor geomechanical quality coupled with controlled blasting activities to improve the excavation performance. In addition, a well defined trend of movement was detected for the MPs along the western border of cut slopes (solid white line, letter E). A small region of movement toward the sensor (possibly uplift) was related to a crushing area (letter F). In N4E mine, blocks of iron ore are transported to the primary crusher, where they are reduced into particles with sizes of 20 mm or less. This is the first stage in the ore processing. A crushing installation was located within the mine at the time of the research. SqueeSAR™ measurements in this area showed dispersed points with irregular deformation profiles, generally defining a very subtle uplift trend (accumulated displacement ~ 6 mm for the period of 20/Mar–10/Aug 2012). The cause of these small displacements is not clear.

For the remainder of the mine, stability was characterized with the dry period based on the LoS deformation maps. Results using the 33 scenes indicated a movement away from the sensor possibly due to settlements on waste pile W with a maximum accumulated displacements of −395.86 mm, displacement rate of −370 mm/year and with few MPs over pile NW-1 showing maximum accumulated displacements of −327.88 mm, displacement rates of −301.70 mm/year. According to Vale, the detected settlements of waste dumps during the time span of the 33 images are expected.

Table 3 reveals interesting relationships of MPs and geomechanical units: (a) the highest amount of MPs was associated with geomechanical classes with the largest areas, but showing the lowest densities (classes IV, V). Both units are related to geomechanical classes with poor quality, and the most intense exploitation (country rock, iron ore), (b) the results of processing using 14 images compared to all data-stack have shown that a total of 216 MPs was lost, and a new distribution of detected PS/DS was obtained, with losses for classes V and IV and increases for classes II and III.

Table 4 presents some quantitative stability results of SqueeSAR™ analysis assuming two intervals of accumulated LoS displacements: (a) indicative of a movement away from the sensor, probably subsidence (< −0.6 cm) and (b) indicative of stability (≤0.6 cm up to

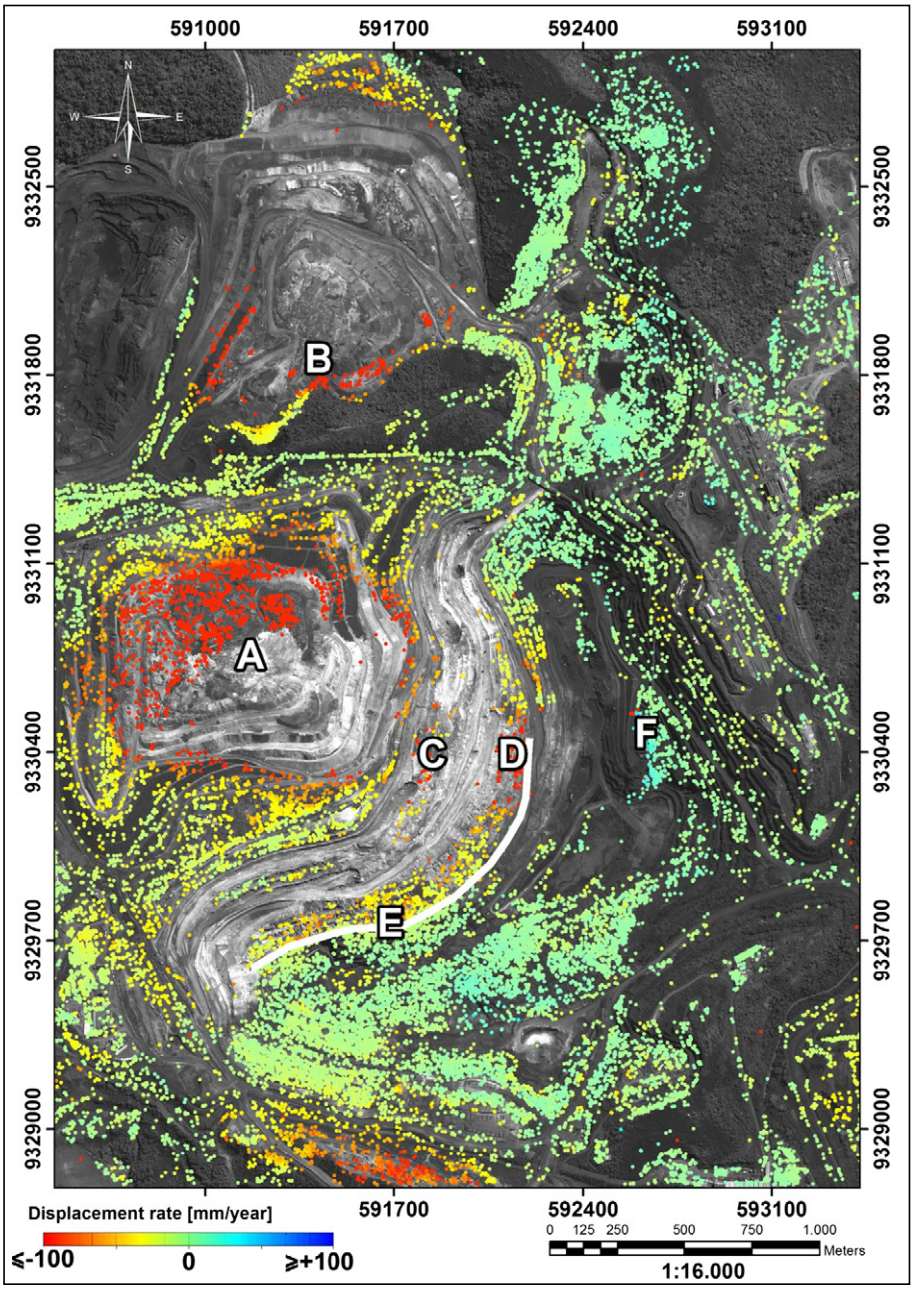

Fig. 10. SqueeSAR™ results for the N4E mine referring to the 20/Mar–10/Aug, 2012 period (14 TSX-1 images). LoS average deformation annual velocities (mm/year) of MPs are color-coded from blue-greenish (stable conditions) to red (a movement away from the sensor, probably corresponding to subsidence). See text.

≥ −0.6 cm). These intervals were chosen taking into account that ±0.6 cm was the standard deviation (1σ) that was obtained from SqueeSAR™ over the corner reflector. Using the first 14 scenes, unstable areas were mainly associated with class IV (22% of MPs), and subordinately with classes V (8% of MPs), II (7% of MPs) and III (4%). These results are compatible with an overall stability of the pit during this period, and instabilities detected for sectors of cut slopes spatially related to units characterized by low geomechanical qualities. In addition, a small cluster of MPs showing accumulated deformation with positive values was detected in the crushing area. When using the 33 images, surface deformations were detected for all classes, and in general, the stability was decreased. A combination of factors can be considered to explain these results: a) the influence of rainfall, b) the minimum accumulated displacement (−0.6 cm) was now detected using a larger time interval, meaning that MPs with subtle subsidence, not previously mapped, were also included, (c) distinct coherence values (MPs with higher coherence

Table 3
Relationship between MPs and Geomechanical classes (N4E mine).

Geomechanical class	Area (km^2)	Number of MPs[a]	MPs/km^2[a]	Number of MPs[b]	MPs/km^2[b]
II (very good rock)	0.4286	2311	5392	2533	5910
III (good rock)	0.3498	1843	5269	2682	7667
IV (poor rock)	2.7013	9438	3494	8913	3299
V (very poor rock)	1.2142	6064	4994	5312	4375

[a] 14 images.
[b] 33 images.

Table 4
Relationship between deformation and geomechanical classes.

Geomechanical class	MPs with displacements indicative of movement away from the sensor[a]	MPs with displacements indicative of stability[a]	MPs with displacements indicative of movement away from the sensor[b]	MPs with displacements indicative of stability[b]
II	172 (7%)	2131 (93%)	921 (36%)	1607 (64%)
III	78 (4%)	1760 (96%)	724 (27%)	1946 (73%)
IV	2086 (22%)	7331 (78%)	2713 (30%)	6124 (70%)
V	508 (8%)	5487 (90%)	1260 (24%)	3987 (75%)

[a] 14 images.
[b] 33 images.

of 0.85 for the first processing and 0.76 for the second one). Finally, the same behavior of movement toward the sensor was detected for MPs in the crushing area using the 33 scenes.

5.3.1. SqueeSAR™ results compared with in situ geotechnical measurements

In an attempt to validate the SqueeSAR™ results with geodetic survey data, total station/prism measurements were used. Five measurement sites were used in this paper and corresponded to data provided by Vale using Leica total station (TCRA 1201 R 1000) from cut slopes of the central pit. The data covered the interval of 03/May 2012 up to 11/Jan 2013, but with a higher temporal frequency (3 to 4 days) compared to the TSX-1 (11 days). To this end, geographic coordinates of both datasets were converted to World Geodetic System—WGS 84, and in order to meet short distance constraint, only MPs located within a distance smaller than 10 m from prisms were used. Finally, considering that prism values were not acquired at the same time at the TSX-1 passes, a resampling process was applied on the prism data based on polynomial interpolation (3rd degree) aiming at predicting field deformation values simultaneously with the SAR measurements.

Since horizontal displacements turned out to be negligible compared to vertical variations, the prism vertical values (Δh) were projected along the satellite LoS by multiplying these values by the cosine of the incidence angle ($\theta = 41.3^{\circ}$). The uncertainties of the calculated LoS-projected vertical prism displacements were estimated based on covariance propagation, which considered components of angular measurements (vertical and azimuth), distances from total station to prisms, error specification of the equipment, number of measurements and geometry of SAR acquisition (Galo and Camargo, 2013). As an example, it was concluded that for a 1000 m total station–prism distance, the expected vertical error in LoS is approximately ± 11 mm for 3σ (99.99% of probability). Thus, variations of Z_{Los} values within this interval (± 11 mm) were interpreted as random errors, while variations outside this interval probably express real deformation. It is important to mention that Vale's Geotechnical team uses a broader interval (± 15 mm in LoS projection) as an alert limit for detection of slope movements. Finally, the nonparametric Wilcoxon test was applied in order to check if SqueeSAR™ measurements provide a similar displacement inference to the prism measurements. The Wilcoxon is a statistical test that compares two paired groups and calculates the difference between each set of pairs. It was used to test the null hypothesis that two populations have the same median value and, therefore, can be considered statistically similar. If this is the case, then the measurement strategy based on SqueeSAR™ may be presumed to be representative of the surface displacement expressed by prism values.

In Fig. 11, the LoS projected deformation of MPs and corresponding prism time series, covering the interval of 253 days (03/May 2012–11 Jan 2013) are superimposed. Based on the prism displacements, it is possible to conclude for an overall stability of the cut slopes, given by the concentration of values within the expected errors bars (theoretical and Vale's limits). Points related to prisms have exhibited a higher dispersion of measurements. This can be explained by several factors including adverse weather conditions (dust and haze during dry and wet seasons impair the visibility among station and prisms), distinct operator teams and interpolation errors. SqueeSAR™ time series showed a good correlation with field information, indicative of stable conditions for the cut slopes. According to the Wilcoxon test, the null hypothesis for each sample pair was accepted (true), with a level of 5% of significance. Unfortunately, it was not possible to have prism measurements covering the end of the rainy season (18/Mar–20/Apr 2013). However, the overall agreement between remote and field information means that SqueeSAR™ analysis is a reliable and powerful way to monitor surface displacement evolution in time, providing data with millimetric accuracy, compatible with in situ geotechnical measurements The lower temporal frequency of SqueeSAR™ when compared to the higher frequency of prism measurements is compensated by the synoptic SAR coverage over a dense grid, providing data independently of field access, and with millimeter accuracy. Therefore, the combination of SqueeSAR™ and prism geotechnical monitoring is an efficient and effective method for monitoring deformation in this environment.

5.3.2. SqueeSAR™ results and geological/geomechanical information

Fig. 12(A) shows the spatial distribution of SqueeSAR™ MPs and lineaments extracted from stereo analysis using RADARSAT-2 data. This analysis is important since it complements the detailed information available only over the pit area. Lineaments were well characterized in the 3D perception and were related to three main regional structures: (a) a N40W system, interpreted as joints/fractures concentrated on the SE border of the pit, where the Carajás Strike–Slip fault system is the most prominent regional feature, (b) a N70E-trending set of lineaments that occurs on the eastern sector of the pit, which is spatially related to the same regional trend that extends from Carajás Complex to Serra Leste, and (c) a NNW system related to strike-slip splay fault component of the sinistral kinematics along Carajás fault.

The spatial relationship of structures with SqueeSAR™ MPs is evident for some sectors of the N4E mine. The lineament, striking E–NE in the center of Fig. 12(B), defines two blocks of MPs: a cluster of stable MPs in the northern sector, and group of MPs in the southern sector exhibiting movement away from the sensor, that could be related to subsidence. Using a GNSS receiver for location, field verification was concentrated on bench walls along the easternmost end of this lineament, and it was possible to characterize weathered mafic rocks interleaved with hematite by a ENE-trending subvertical faults (Fig. 12 C). The mechanism on how this structure has controlled the distribution of MPs with distinct displacement patterns is not clear. However, the spatial relationship is unequivocal, and suggests that faults in the contact of distinct geomechanical classes could be acting as barriers in the spatial distribution of MPs, separating stable from subsiding terrains. Two additional aspects also favor instabilities in the area: the presence of a shear system dipping toward the center of the pit (BVP, 2011), and blasting activities to increase in-pit comminution and excavation performance, particularly on the southern block (the location of a drilling machine operating in October 2012 is indicated in Fig. 12B).

5.4. Speckle Tracking (ST)

Due to intense ongoing mining exploitation, surface deformation and slope stability are very important issues for the waste dumps in Carajás. In order to test ST technique, the NW-1 waste pile was selected. This manmade structure with 33-year-age is a valley-fill dump

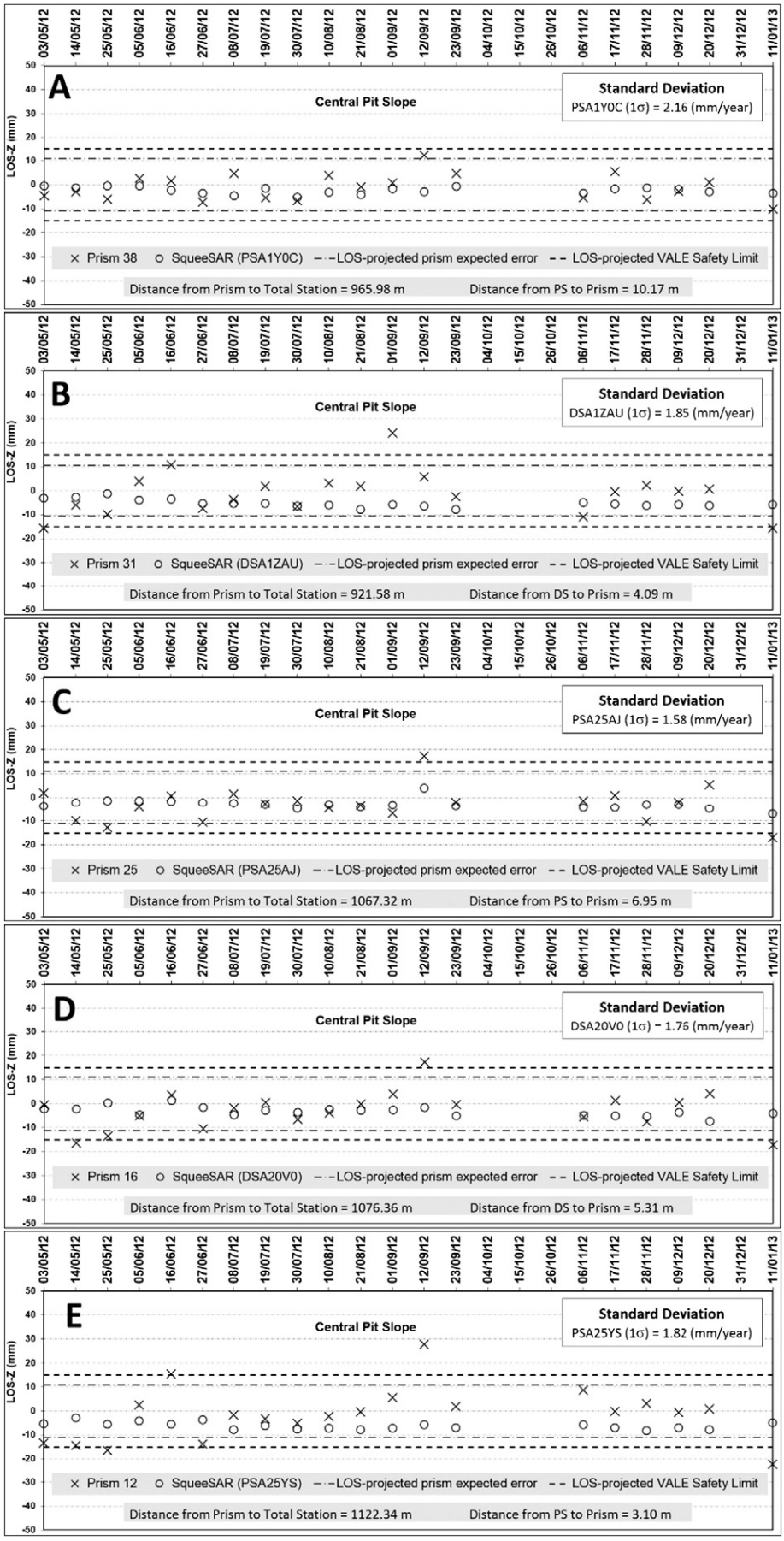
A
Central Pit Slope
Standard Deviation
PSA1Y0C (1σ) = 2.16 (mm/year)
LOS-Z (mm)
Prism 38
SqueeSAR (PSA1Y0C)
LOS-projected prism expected error
LOS-projected VALE Safety Limit
Distance from Prism to Total Station = 965.98 m
Distance from PS to Prism = 10.17 m
B
Central Pit Slope
Standard Deviation
DSA1ZAU (1σ) = 1.85 (mm/year)
LOS-Z (mm)
Prism 31
SqueeSAR (DSA1ZAU)
LOS-projected prism expected error
LOS-projected VALE Safety Limit
Distance from Prism to Total Station = 921.58 m
Distance from DS to Prism = 4.09 m
C
Central Pit Slope
Standard Deviation
PSA25AJ (1σ) = 1.58 (mm/year)
LOS-Z (mm)
Prism 25
SqueeSAR (PSA25AJ)
LOS-projected prism expected error
LOS-projected VALE Safety Limit
Distance from Prism to Total Station = 1067.32 m
Distance from PS to Prism = 6.95 m
D
Central Pit Slope
Standard Deviation
DSA20V0 (1σ) = 1.75 (mm/year)
LOS-Z (mm)
Prism 16
SqueeSAR (DSA20V0)
LOS-projected prism expected error
LOS-projected VALE Safety Limit
Distance from Prism to Total Station = 1076.36 m
Distance from DS to Prism = 5.31 m
E
Central Pit Slope
Standard Deviation
PSA25YS (1σ) = 1.82 (mm/year)
LOS-Z (mm)
Prism 12
SqueeSAR (PSA25YS)
LOS-projected prism expected error
LOS-projected VALE Safety Limit
Distance from Prism to Total Station = 1122.34 m
Distance from PS to Prism = 3.10 m

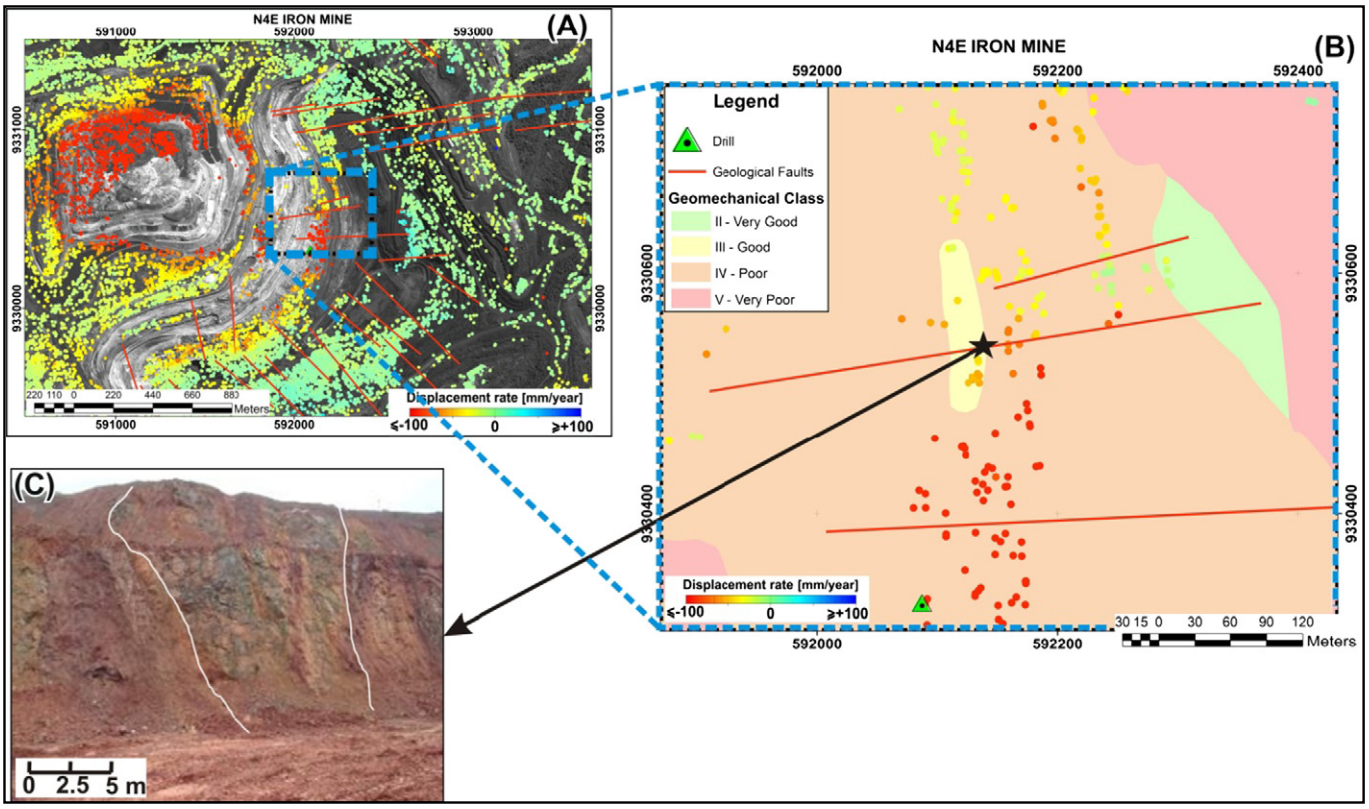

Fig. 12. SqueeSAR™ MPs velocities (mm/year) for the period of 20/Mar–10/Aug 2012 plotted on mapped RST-2 UF geological structures representing fractures and faults (A). The small rectangle (blue) corresponds to the map (B) depicting the spatial relationships of MPs and geomechanical units. Field picture showing the contact of hematite and mafic by E–NE trending vertical fault (C).

configuration, reaching 220 m total height, with 20 m bench height, 10 m berm width, and 27° of overall slope angle (crest-to-toe). The intense activities on the pile can be reflected by the absence of PS/DS measurements using SqueeSAR™ analysis. Due to the operational conditions, in situ measurements, which could reveal temporal changes of the topography, are not systematically acquired for the same locations. Topographic measurements are carried out for restricted sectors, depending on the changes of the topography due to the ongoing operations. Thus, this information has shown to be impractical to be used as validation, since the updated measurements are variable in time and space. Only two sets of field elevation measurements were used in this investigation and are related to Vale's topographic surveys dated on 20/Mar and 13/Jul, 2012 (Fig. 13 A). The results of ST analysis using 11 TSX-1 images (20/Mar–08/Jul, 2012) have shown MPs covering large areas within the waste dump, and have highlighted the improvement that was achieved as compared to SqueeSAR™ (Fig. 13 B and C).

Higher magnitudes of displacements (maximum = −47.72 cm) and deformation rates (maximum = −126.55 cm/year) were detected related to settlements along this profile AB. Areas without information are associated to very intense surface changes; here no SAR-based displacement measurement was possible. Fig. 14(A) presents the comparison of profiles from ST (Profile AB from Fig. 13(C)) and LoS-projected elevation values of reflecting prisms covering two closer periods in 2012 (20/Mar–08/July for ST, 20/Mar–13/Jul for prisms). The analysis of this figure shows a good match of the profiles, depicting the elevation variations and the absence of ST information, when intense mining operation is dominant. Fig. 14(B) shows the ST results regarding settlement differences for measured period. It is important to mention that systematic information of settlement values for waste piles in Carajás is not available. Thus, this innovative ST approach opens real perspectives for operational monitoring of these manmade mining structures.

6. Concluding remarks

In this investigation, the capabilities, potential and limitations of an integrated SAR analysis for monitoring surface displacements of mining structures of open pit iron mines of Carajás were demonstrated. A stack of 33 TSX-1 images was analyzed and different SAR techniques were combined in order to extract the maximum information content about ground displacements and surface changes. Due to the complexity of this environment, an integrated SAR analysis was designed to monitor over time distinct deformation regimes, ranging from low (millimeter) to high (m) displacement rates, and to map changes affecting the area of interest by using amplitude data only. The following aspects can be highlighted:

- SqueeSAR™ data have provided a synoptic and informative view of the deformation processes affecting the Carajás complex. Deformation maps showed that most of the mining complex was stable during the time span of the TSX-1 coverage, but high deformation rates were detected over waste dumps and some pit slopes (N4E mine). For the main mining infrastructure (dam, railway, road access), the values are indicative of stability. In addition, the highest amount of MPs for N4E mine was associated with geomechanical classes showing poor

Fig. 11. Temporal evolution of the LoS-projected deformation for five reflecting prisms (A to E) and corresponding SqueeSAR™ measurements on the central pit slopes. Each plot shows the bars of the expected vertical LoS-projected error of prism (3σ) and the Vale's alert limit for deformation, the distances from PS/DS to prisms, and the distance from prisms to total station.

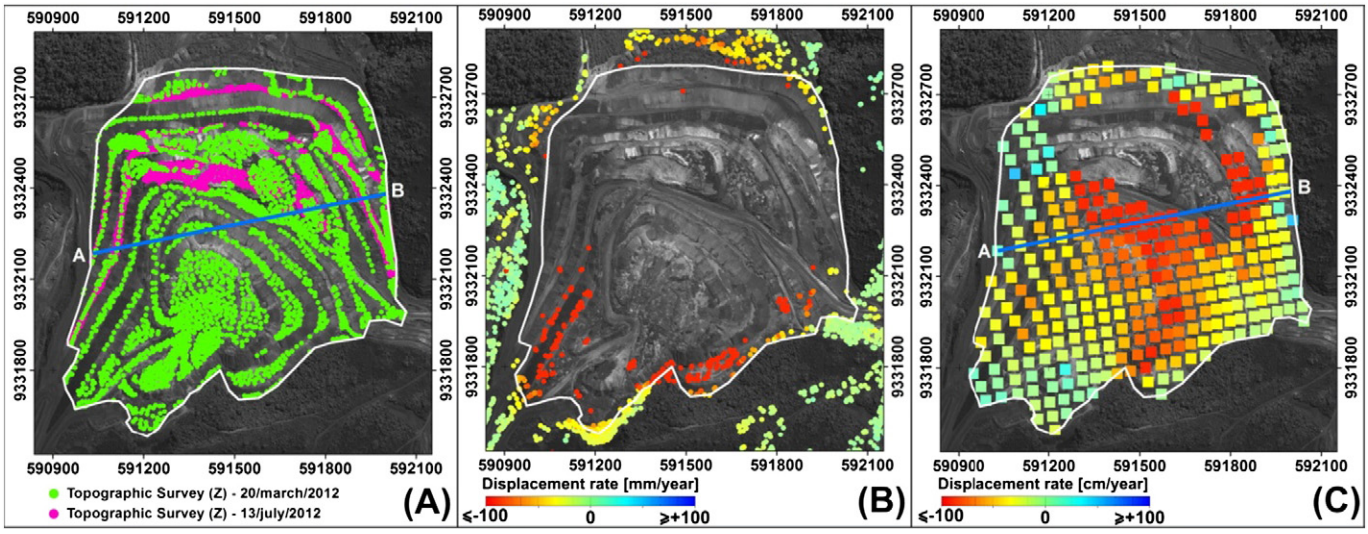

Fig. 13. Waste pile NW-1 showing: (A) Field elevation measurements (total station/prism) related to topographic surveys during 2012. Green dots correspond to sites where no elevation measurement was done since 20/Mar because no mining activities were carried out. Rose dots correspond to points where elevation was measured due to mining operations during the period of 20/Mar–13/Jul 2012; (B) SqueeSAR™ result (14 scenes) showing the absence of PS/DS measurements within the pile; (C) ST result showing LoS-projected displacements for the time interval of 20/Mar–08/July, 2012. The profiles are discussed in the text.

quality. When using the total stack of 33 images in the interferometric processing, rather than the subset of images of the dry period, a lower number of MPs were obtained due to the loss of temporal coherence (intense precipitation, high displacement rate, rapidly changing environment).

- Geodetic survey data using total station/prism measurements were important for the validation of SqueeSAR™ measurements. A good agreement was obtained in the comparison between the two sources of independent data measuring the same conditions (time, place) of slope stability. This confirms that SqueeSAR™ data can be used for deformation monitoring and risk assessment, providing high accuracy of displacement data, over a dense grid of MPs and large areas.
- Our research suggests that geological structures play a key role in controlling the rock unit displacements expressed by distinct

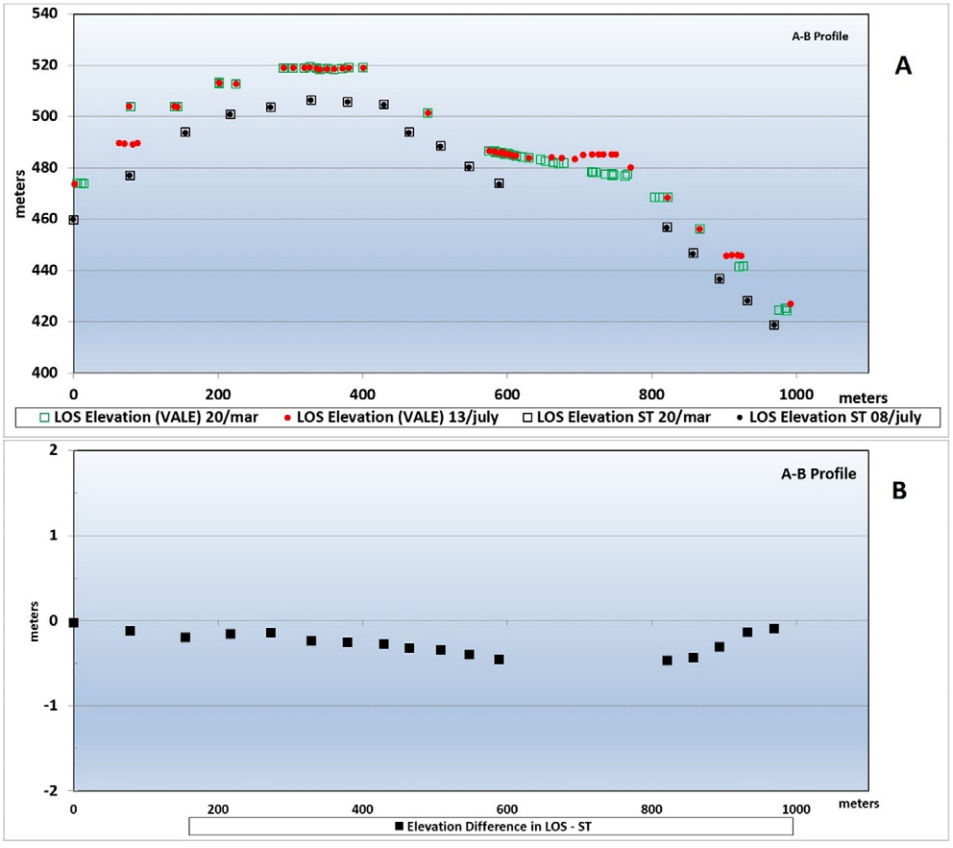

Fig. 14. AB profiles of settlements extracted from ST and total station/prisms (A), differences of settlements by ST technique for the period of 20/Mar–08/Jul, 2012 (B).

spatial distribution and displacement values of SqueeSAR™ MPs in N4E mine. An additional effort is necessary to clarify these relationships.

- ST has provided displacement time series in areas characterized by fast deformation, not detected by SqueeSAR™. Amplitude change detection can be used to track changes in areas where no SqueeSAR™ and/or ST measurements are feasible.
- A complementary and synergistic use of space-based SAR information with field monitoring system information proved to be fundamental for operational perspective.
- In order to fully exploit the potentiality of the proposed approach, the usage of ascending and descending SAR passes is necessary in order to minimize lack of information due to radar foreshortening, to get redundancy in case of acquisition failures and to get horizontal and vertical deformation components.
- Regarding limitations of the integrated approach, since the techniques depend on the sequential acquisitions, the information is not real time. Its effectiveness is limited over areas showing low coherence, such as rapidly changing surfaces. Finally, two important cost factors to be considering are the acquisition of a large number of SAR images for the interferometric processing, and the necessity of an updated high-resolution DEM to remove the topographic phase component (that, although not strictly necessary, can speed up the processing and minimize the number of satellite data necessary to obtain reliable information).
- The integrated SAR analysis can provide long-term monitoring and predictive solutions for in-pit mining operations, waste piles and other surface assets without the need for ground instrumentation. Reporting on open pit monitoring programs can be implemented on two time scales. The first is a situation report weekly, monthly or even after each new data acquisition using unwrapped interferograms and changed detection map. The second time scale is quarterly, 6-month or annual analysis performed with SqueeSAR™ and ST technologies providing a full deformation history over thousands of sample points.
- In the future, the synergistic use of different satellite SAR sensors operating at different frequencies (Sentinel-1A/B, ALOS-2, TSX, COSMO-SkyMed, RADARSAT Constellation Mission) will allow an almost daily acquisition of satellite data over an area of interest, opening the way to new and effective monitoring systems. Meanwhile, the combined use of satellite and in situ observations appears to be the best way to monitor mining areas, improving both the understanding of the phenomena affecting the mine and the safety of both workers and local infrastructures. This can be done already today and should be adopted in many other mining districts, not only in South America.

Acknowledgments

This investigation was carried out under the scope of a FAPESP-Vale-INPE project (Process no. 2010/51267-9). The authors would like to thank Vale S.A. for providing access to geological, geomechanical and field deformation data, and CNPq for a grant received by the first author (Proc. # 304254/2009-6). The authors are particularly grateful to the Geotechnical Vale's team in Carajás for the support during field campaigns, and to Henry Galbiatty (Vale S.A.) for his continuous help to the research in Carajás. The paper benefited significantly from the journal's reviewers.

References

Beisiegel, V.R., Bemardelli, A.L., Drummond, N.F., Ruff, A.W., Tremaine, J.W., 1973. Geologia e recursos minerais da Serra dos Carajás. Braz. J. Geosci. 3 (4), 215–242.

Bieniawski, Z.T., 1989. Engineering Rock Mass Classifications. John Wiley & Sons, New York (272 pp.).

BVP, 2011. Lithostructural and lithogeomechanical mapping of the N4E mine. BVP Engenharia Internal Report ((ref: VL 070-10-E-CA-RT-03-037-00), 80 pp.).

Colesanti, C., Ferretti, A., Novali, F., Prati, C., Rocca, F., 2003. Monitoring of progressive and seasonal ground deformation. IEEE Trans. Geosci. Remote Sens. 41 (7), 1685–1701.

Colesanti, C., Mouelic, S.L., Bennani, M., Raucoules, D., Carnec, C., Ferretti, A., 2005. Detection of mining related ground instabilities using the permanent scatterers technique: a case study in the east of France. Int. J. Remote Sens. 26 (1), 201–207.

Crosetto, M., Crippa, B., Biescas, E., 2005. Early detection and in-depth analysis of deformation phenomena by radar interferometry. Eng. Geol. 79 (2005), 81–91.

Ferretti, A., 2014. Satellite InSAR Data: Reservoir Monitoring From Space, European Association of Geoscientists & Engineers. EAGE publishers (140 pp., e-book at http://bookshop.eage.org/webshop/product_details.aspx?prod_code=AA0232).

Ferretti, A., Prati, C., Rocca, F., 2000. Nonlinear subsidence rate estimation using permanent scatterers in differential SAR interferometry. IEEE Trans. Geosci. Remote Sens. 38 (5), 2202–2212.

Ferretti, A., Prati, C., Rocca, F., 2001. Permanent scatterers in SAR interferometry. IEEE Trans. Geosci. Remote Sens. 39 (1), 8–20.

Ferretti, A., Monti-Guarnieri, A., Prati, C., Rocca, F., Massonnet, D., 2007. InSAR Principles: Guidelines for SAR Interferometry Processing and Interpretation. ESA Publications, TM-19 92-9092-233-8 (Available at: http://www.esa.int/About_Us/ESA_Publications).

Ferretti, A., Fumagalli, A., Novali, F., Prati, C., Rocca, F., Rucci, A., 2011. A new algorithm for processing interferometric data-stacks: SqueeSAR™. IEEE Trans. Geosci. Remote Sens. 49 (9), 3460–3470.

Gabriel, A.K., Goldstein, R.M., Zebker, H.A., 1989. Mapping small elevation changes over large areas: differential radar interferometry. J. Geophys. Res. 94 (B7), 9183–9191.

Galo, M., Camargo, P.O., 2013. Analysis of the expected errors of reflecting prisms in the N4E mine. Project FAPESP # 2010/51267-9, Internal Report 8 pp.

Hartwig, M.E., Paradella, W.R., Mura, J.C., 2013. Detection and monitoring of surface motions in active mine in the Amazon region, using persistent scatterer interferometry with TerraSAR-X satellite data. Remote Sens. 5, 4719–4734.

Hawley, M., Marisett, S., Beale, G., Stacey, P., 2009. Performance assessment and monitoring. In: Read, J., Stacey, P. (Eds.), Guidelines for Open Pit Slope Design. CRC Press, Balkema, The Netherlands, pp. 327–379.

Herrera, G., Tomás, R., Lopez-Sanchez, J.M., Delgado, J., Mallorqui, J.J., Duque, S., Mulas, J., 2007. Advanced DInSAR analysis on mining areas: La Union case study (Murcia, SE Spain). Eng. Geol. 90, 148–159.

Herrera, G., Tomas, R., Vicente, F., Lopez-Sanches, J.M., Mallorquí, J.J., Mulas, J., 2010. Mapping ground movements in open pit mining areas using differential SAR interferometry. Int. J. Rock Mech. Min. Sci. 47 (2010), 1114–1125.

Holdsworth, R., Pinheiro, R.V.L., 2000. The anatomy of shallow-crustal transpressional structures: insights from the Archean Carajás fault zone, Amazon, Brazil. J. Struct. Geol. 22, 1105–1123.

Horbe, A.M.C., Costa, M.L., 2005. Lateritic crusts and related soils in eastern Brazilian Amazonia. Geoderma 126 (2005), 225–239.

IBRAM, 2013. Information and Analysis on the Brazilian Mineral Economy. 7th edition. Brazilian Mining Association (web site: www.ibram.org.br (accessed in January 2014)).

ISRM, 1981. Rock Characterization, Testing and Monitoring Suggested Methods. Pergamon Press, London 211 pp.

Jaroz, A., Wanke, D., 2003. Use of InSAR for monitoring of mining deformations. Proceedings of the Fringe Workshop 2003, Frascati, Italy, 1–5 December 2003 (ESA SP-550, June 2004).

Kääb, A., 2005. Remote sensing of mountain glaciers and permafrost creep. Schriftenreihe Physische Geographie 48 3 85543 244 9 266 pp.

Meireles, E.M., Hirata, W.K., Amaral, A.F., Medeiros Filho, C.A., Gato, W.C.A., 1984. Geologia das Folhas Carajás e Rio Verde, Província Mineral dos Carajás, Estado do Para. Annals 31 Brazilian Geological Congress, Rio de Janeiro, pp. 2164–2174.

Ng, A.-H.M., Ge, L., Yan, Y., Li, X., Chang, H.-C., Zhang, K., Rizos, C., 2010. Mapping accumulated mine subsidence using small stack of SAR differential interferograms in the Southern coalfield of New South Wales, Australia. Eng. Geol. 115, 1–15.

Oliveira, C.G., Paradella, W.R., Silva, A.Q., 2011. Assessment of radargrammetric DSMs from TerraSAR-X stripmap images in a mountainous relief area of the Amazon region. ISPRS J. Photogramm. Remote Sens. 66, 67–72.

Orman, M., Peevers, R., Sample, K., 2011. Waste piles and dumps. SME Mining Engineering Handbook 3rd ed. SME, Englewood, CO, USA, pp. 667–680 (Vol. 1).

Paradella, W.R., Cheng, P., 2013. Using GeoEye-1 stereo data in mining application: automatic DEM generation. Geoinformatics 16 (January/February), 10–12.

Paradella, W.R., Silva, M.F.F., Rosa, N.A., Kushigbor, C.A., 1994. A geobotanical approach to the tropical rain forest environment of the Carajás mineral province (Amazon region, Brazil), based on digital TM-Landsat and DEM data. Int. J. Remote Sens. 15 (8), 1633–1648.

Paradella, W.R., Bignelli, P.A., Veneziani, P., Pietsch, R.W., Toutin, T., 1997. Airborne and spaceborne Synthetic Aperture Radar (SAR) integration with Landsat TM and gamma ray spectrometry for geological mapping in a tropical rainforest environment, the Carajás mineral province, Brazil. Int. J. Remote Sens. 18 (7), 1483–1501.

Perski, Z., Hanssen, R., Wojcik, A., Wojciechowski, T., 2009. InSAR analyses of terrain deformation near the Wieliczka Salt Mine, Poland. Eng. Geol. 106, 58–67.

Raspini, F., Moretti, S., Fumagalli, A., Rucci, A., Novali, F., Ferretti, A., Prati, C., Casagli, N., 2014. The COSMO-SkyMed constellation monitors the Costa Concordia wreck. Remote Sens. 6, 3988–4002.

Rignot, E.J.M., van Zyl, J.J., 1993. Change detection techniques for ERS-1 SAR data. IEEE Trans. Geosci. Remote Sens. 31 (4), 896–906.

Rucci, A., Vasco, D.W., Novali, F., 2013. Monitoring the geologic storage of carbon dioxide using multicomponent SAR interferometry. Geophys. J. Int. 193 (1), 197–208.

Sá, G., 2010. Caracterização litoestrutural e parametrização geomecânica das superfícies de rupturas em taludes da Mina N4E, Carajás, Pa. Thesis for the Master Degree in Geotechnical Engineering. Federal University of Ouro Preto 172 pp.

Santos, A.R., Paradella, W.R., Veneziani, P., Morais, M.C., 1999. A esteroscopia com imagens RADARSAT-1: uma avaliação geológica na Província Mineral de Carajás. Rev. Bras. Geociênc. (Braz. J. Geosci.) 29, 623–628.

Scheuchl, B., Ullmann, T., Koudogbo, F., 2009. Change detection using high resolution TERRASAR-X data: preliminary results. ISPRS Hannover Workshop 2009: High-Resolution Earth Imaging for Geospatial Information, 2–5 June 2009, Hannover, Germany.

Silva, A.Q., Paradella, W.R., Freitas, C.C., Oliveira, C.G., 2009. Relationship between PALSAR backscatter and surface-roughness parameter from iron laterites in Carajás, Amazon Region. IEEE Trans. Geosci. Remote Sens. 47, 4027–4031.

Tao, C.V., Hu, Y., 2001. A comprehensive study of the rational function model for photogrammetric processing. Photogramm. Eng. Remote Sens. 67 (12), 1347–1357.

Tassinari, C.C.G., Macambira, M., 2004. A evolução tectônica do Craton Amazônico. In: Mantesso-Neto, V., Bartorelli, A., Carneiro, C.D.R., Brito Neves, B.B. (Eds.), Geologia do Continente Sul Americano: Evolução da obra de Fernando Flávio Marques Almeida, pp. 471–486.

Vale, 2012. Geotechnical monitoring with Slope Stability Radar: SW flank, N4E mine. Internal Vale's report, GAGHN/GEDEN, September, 2012 8 pp.

Vale, 2013. Geotechnical monitoring with slope stability radar: central pit, N4E mine. Internal Vale's report, GAGHN/GEDEN, March, 2013 5 pp.

Vaziri, A., Moore, L., Ali, H., 2010. Monitoring systems for warning impending failures in slopes and open pit mines. Nat. Hazards 55, 510–512.

Veneziani, P., Santos, A.R., Paradella, W.R., 2004. A evolução tectono-estratigráfica da Província Mineral de Carajás: um modelo com base em dados de sensores remotos orbitais (SAR-C RADARSAT-1, TM LANDSAT-5), aerogeofísica e dados de campo. Rev. Bras. Geociênc. (Braz. J. Geosci.) 34, 67–78.

Wegmuller, U., Strozzi, T., Benecke, N., Petrat, L., Schlautmann, M., Kuchenbecker, R., Deutschmann, J., Spreckels, V., Schafer, M., Busch, W., Schade, M., Paar, W., Maly, R., Staisch, H., Hoffmann, F., Al-Enezi, A., 2007. Monitoring mining induced ground-movements using SAR interferometric techniques. Proceedings of Envisat Symposium, Montreaux, Switzerland, 23–27 April, 2007 (ESA SP-636) 5 pp.